



Universiteit Utrecht

Opleiding Natuur- en Sterrenkunde

Effects of artificial snow cover on the mass balance of the Morteratsch glacier

BACHELOR THESIS

Jos Veenhoven



Supervisors:

Dr. CARLEEN TIJM-REIJMER
IMAU

Prof. Dr. HANS OERLEMANS
IMAU

January 2020

Abstract

The glacier Vadret da Morteratsch has been losing mass rapidly in the past century. A proposed solution to its retreat is the deposition of artificial snow made from meltwater to the glacier surface. The effects of this solution are analyzed using a mass and energy balance model of the Morteratsch glacier. The model uses input from nearby weather stations and is tuned using data from the Automatic Weather station on the glacier. In the reference run, three mass balance years from 2016-2019 are analyzed. During this period, the modelled mass balance of Morteratsch glacier is $-0,80$ m w.e./yr. In the experimental runs, artificial snow is deposited to the glacier surface for wet bulb temperatures below -2 °C. The artificial snow supply is constrained to an area of $0,8$ km² on the glacier tongue. When there are no limitations to the amount of water used, the glacier mass balance can be increased to $+0,14$ m w.e./yr with artificial snow deposition in this area. In practice, it is uncertain whether enough meltwater can be stored throughout the year. If artificial snow supply is constrained by a water reservoir of 10^6 m³, the mass balance becomes -0.42 m w.e./yr. Running the model with a reservoir of 10^4 m³ results in a mass balance of -0.68 m w.e./yr.

Cover: The Morteratsch glacier (right) and Pers glacier (left) in August 2017. Photo made from a glider by C. Levy, Academia Engiadina.

Contents

1	Introduction	1
2	Background	3
2.1	Glacier basics	3
2.1.1	Mass balance	4
2.1.2	Energy balance	4
2.2	The Morteratsch glacier	6
2.2.1	Observations at the Morteratsch glacier	7
2.3	MortAlive project	9
3	Modelling the Morteratsch glacier	11
3.1	Input & evaluation data	11
3.2	Simulating the snowpack	13
3.2.1	Snowfall	13
3.2.2	Snow density	14
3.2.3	Glacier heat flux	15
3.2.4	Water percolation	15
3.3	Surface energy fluxes	16
3.3.1	Incoming shortwave radiation	16
3.3.2	Albedo	17
3.3.3	Outgoing longwave radiation	18
3.3.4	Incoming longwave radiation	18
3.3.5	Turbulent fluxes	18
3.4	Mass balance	19
4	Evaluating the model	20
4.1	Model tuning	20
4.1.1	Temperature	20
4.1.2	Relative humidity	21
4.1.3	Precipitation	22
4.1.4	Incoming shortwave radiation	22
4.1.5	Incoming longwave radiation	24
4.1.6	Albedo	24
4.2	Model evaluation	25
4.2.1	Comparison with Klok and Oerlemans	27
4.3	Reference run	27
4.4	Model sensitivity	30
4.4.1	Climate sensitivity	30
4.4.2	Parameter sensitivity	31
4.4.3	Other sensitivities	32
5	Experiments and results	33
5.1	Experiments description	33
5.2	Results	33
5.2.1	Height dependence on artificial snow effects	33
5.2.2	Effects of snow on selected area	34

5.2.3	Area variability	36
5.2.4	Water availability constraints	37
5.2.5	Snow supply sensitivity	38
5.2.6	Climate sensitivity	40
6	Conclusions, discussion, and outlook	41
6.1	Key assumptions and model improvements	41
6.2	Main conclusions and future research	42

1 Introduction

Human-induced climate change has many transformative impacts on the earth's landscape. Among the most visible impacts of climate change is global glacier retreat. A well known consequence of melting glaciers is global sea level rise. Together, all valley glaciers lost 220 gigatonnes of mass per year between 2005 and 2016 [1]. This mass loss caused an increase in sea level of 0.61 mm/yr, comparable to the separate contributions of the Greenland and Antarctic Ice Sheet [1]. Glacier retreat also has many local consequences, including decreased stability of mountain slopes and an increase of avalanche frequency [2].

One of the most well studied glaciers in the Eastern Alps is Vadret da Morteratsch, an alpine glacier located in the southeast of Switzerland. The glacier is currently 5.8 km long, but it has lost 2.8 km of its length since recording began in 1887 [3]. The glacier front has retreated to a higher altitude and is not visible anymore from most of the valley. The retreat of the Morteratsch glacier is unfortunate for the local community, whose economy largely depends on glacier related tourism.

Prof. dr. Hans Oerlemans and dr. Felix Keller have been conducting research on Vadret da Morteratsch for a long time [4][5][6]. Together, they have started the project MortAlive, with which they aim to slow down the retreat of the Morteratsch glacier. Their proposed solution for the retreat is covering a part of the Morteratsch glacier with artificial snow made from meltwater. The technology used to produce the snow is based on snow lances, which are already used in the ski industry.

An artificial snow cover acts as a sort of shield for the glacier ice. When the glacier is covered with a snow layer, the incoming energy flux causes some of the snow to melt, protecting the ice underneath as long as the snow is thick enough. But using snow has another advantage: because snow reflects more solar radiation than ice, the incoming energy flux gets decreased, slowing the melt rate of the glacier [5].

In a 2017 study, Oerlemans, Haag and Keller researched how permanently covering a part of the glacier tongue with artificial snow would change the glacier length [4]. The study included an ice flow model of the Morteratsch glacier. Mass balance (average mass loss or gain) at the flow line was used as input. The artificial snow cover was simulated by setting the mass balance to zero at the selected area. The study found that the retreat of the Morteratsch glacier could be decreased with 0.5 km after 20 years of artificial snow supply if the Paris Climate Agreement becomes reality [4].

Since the 2017 study, some questions are left unanswered. The mass balance used as the input was a simple estimation. In my research, I aim to find the mass balance of the Morteratsch glacier and how it changes with artificial snow cover. For this, I use a hypsometric model of the glacier that uses input data from weather stations to simulate the snowfall and energy balance to calculate the mass balance. In the model, I can add artificial snow at any chosen location and find its impacts on the glacier mass balance. I will research how the impact of artificial snow on the mass balance varies with altitude. Then, I will assess where and when the Morteratsch glacier can realistically be covered with artificial snow, taking into account situational and water availability constraints. Finally, I will study the sensitivity of the model results to climate and snow supply variability.

In section 2, I will discuss some background on glaciers. I discuss the Morteratsch glacier and the MortAlive project in particular. In section 3, I explain the most important aspects of the model I used. Section 4 expands on section 3 by discussing how the model was tuned to observational data. Then, I show results of the reference run without artificial snow and discuss the climate and parameter sensitivities of the model. In section 5, I explain the experiments I conducted with the artificial snow and show the results. The implications of the research are discussed in section 6.

2 Background

2.1 Glacier basics

Glaciers are large moving bodies of ice on land. They form in places where more snow falls than melts away over many years. As snow accumulates on a glacier, the lower layers of snow slowly get compressed and most of the air escapes. In addition, a part of the snowpack can melt, percolate into the snowpack, and refreeze later. These processes happen many times, eventually producing firn: a substance much denser than fresh snow. Eventually, through more compression and re-freezing, the firn turns into glacial ice [7].

The process of mass being added to the glacier is referred to as accumulation. Most accumulation consists of snowfall, but glaciers can also gain mass when rain or meltwater (re)freezes inside the snowpack. Loss of mass through melting and sublimation is called ablation. The conditions necessary to form a glacier tend to hold in cold places with sufficient precipitation. Of all glacier mass, the vast majority is located in the Greenland and Antarctic Ice Sheets. Most other glaciers lie in high mountain areas. Although only a fraction of the glacier mass is stored outside Greenland and Antarctica, these glaciers currently contribute to about 34% of all glacial sea level rise [1]. The short term contribution of these glaciers to sea level rise is so significant because they are located in relatively warm areas, which makes them more vulnerable to small changes in the climate [7]. Glaciers move over the underlying terrain because of the gravitational force acting on them. When glaciers are thick enough, the pressure on the lowest layers is so high that it starts to behave like a fluid. In glaciers at relatively higher temperatures, the flow is enhanced by the presence of meltwater in between the terrain and glacier [7].

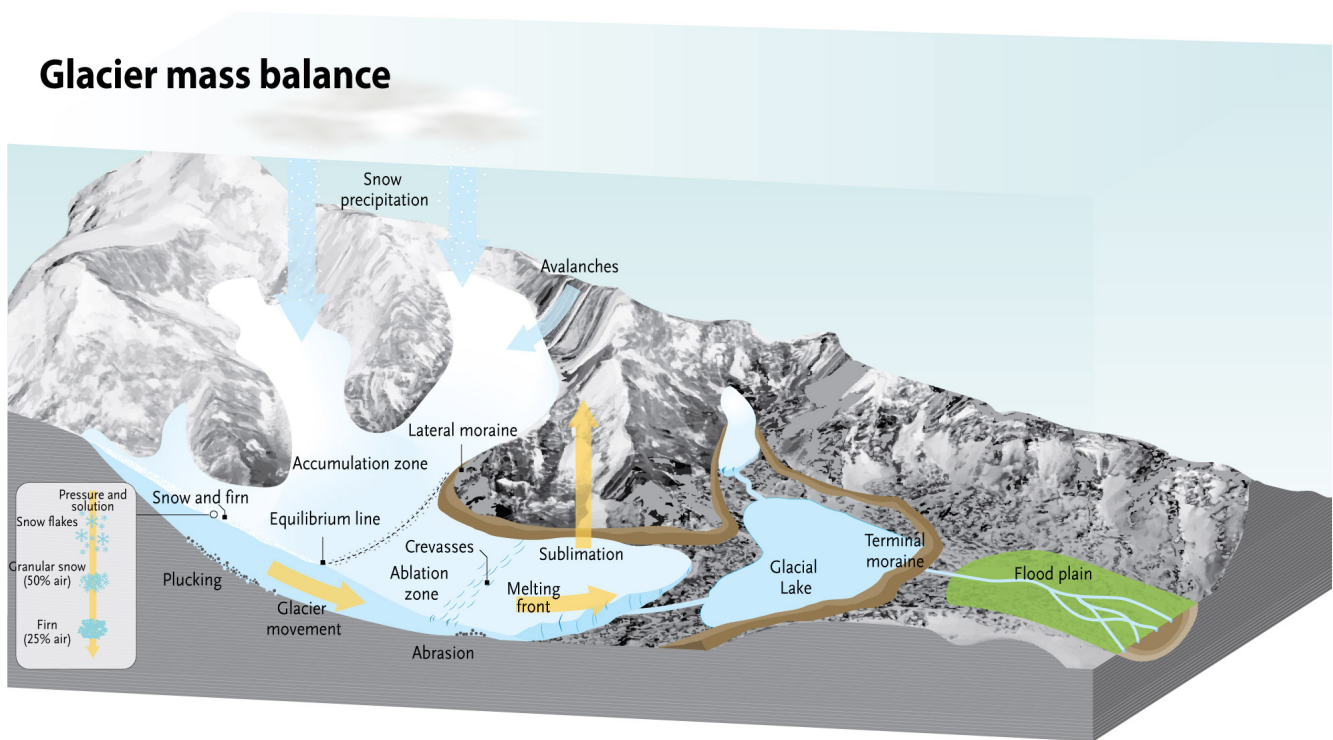


Figure 1: Schematic picture of a glacier by Riccardo Pravettoni [8].

2.1.1 Mass balance

There are different ways to get an indication of the evolution of a glacier over time. Glacier length is one such indication that is relatively easy to measure. Length measurements give a clear sign on whether a glacier is gaining or losing mass. However, focusing only on glacier length can give an incomplete view of the state of the glacier, as it doesn't measure the change in glacier thickness. It is also insufficient if one is interested in the contribution to sea level rise. A more complete view can be obtained by evaluating the change in mass. The mass balance B is the average glacier mass gain or loss caused by accumulation and ablation over a certain period. As an equation, it reads:

$$B = \int (P + M + R + S)dt. \quad (1)$$

Here, P is the snow accumulation rate, M the melt rate R the refreezing rate and S the (de)sublimation rate. P and R cause mass gain, so are always positive. M is always negative. The mass balance is expressed in mass per unit area over a certain time, usually a year. A unit that is often used is meter water equivalent (m w.e.), which is equal to 1000 kg/m².

The mass balance evaluated over each unit area of the glacier is called the specific mass balance. The specific mass balance usually varies significantly over the glacier. On the highest parts of the glacier, the specific mass balance is positive because there is more accumulation than ablation. This area is called the accumulation zone. Although accumulation needs to exceed ablation for a glacier to be formed, glaciers also have an ablation zone, where the specific mass balance is negative. Ablation zones exist because of the flow of ice from higher altitudes. The accumulation and ablation zone are separated by the equilibrium line, where accumulation equals ablation [7]. The average height of the equilibrium line is called the Equilibrium Line Altitude (ELA). The accumulation zone, ablation zone and Equilibrium Line are illustrated in Fig. 1.

Currently, almost all glaciers have a negative total mass balance as a consequence of climate change. The average mass balance of mountain glaciers outside of polar regions was -0.49 m w.e./yr from 2006-2015 [2]. In the Alps, average mass balance is even more negative [2]. In practice, a negative mass balance means that the accumulation zone decreases and the ablation zone increases, resulting in a higher Equilibrium Line and glacier retreat.

2.1.2 Energy balance

The current negative mass balance of many glaciers is the result of increased ablation. Melt increases when energy fluxes towards the glacier surface increase. All energy fluxes are shown in Fig. 2. F is the sum of all surface radiation and heat fluxes, defined to be positive when it is directed towards the glacier. It is given by the following equation:

$$F = S_{in} - S_{out} + L_{in} - L_{out} + Q_L + Q_H \quad (2)$$

Here, S_{in} and S_{out} are the incoming and reflected shortwave radiation. Incoming shortwave radiation is all the solar radiation that reaches the glacier surface. Not all of that radiation is absorbed by the surface. The reflected solar radiation S_{out} is determined by the albedo α of the surface, defined as $\alpha = S_{out}/S_{in}$. The net shortwave flux towards the surface is thus equal to

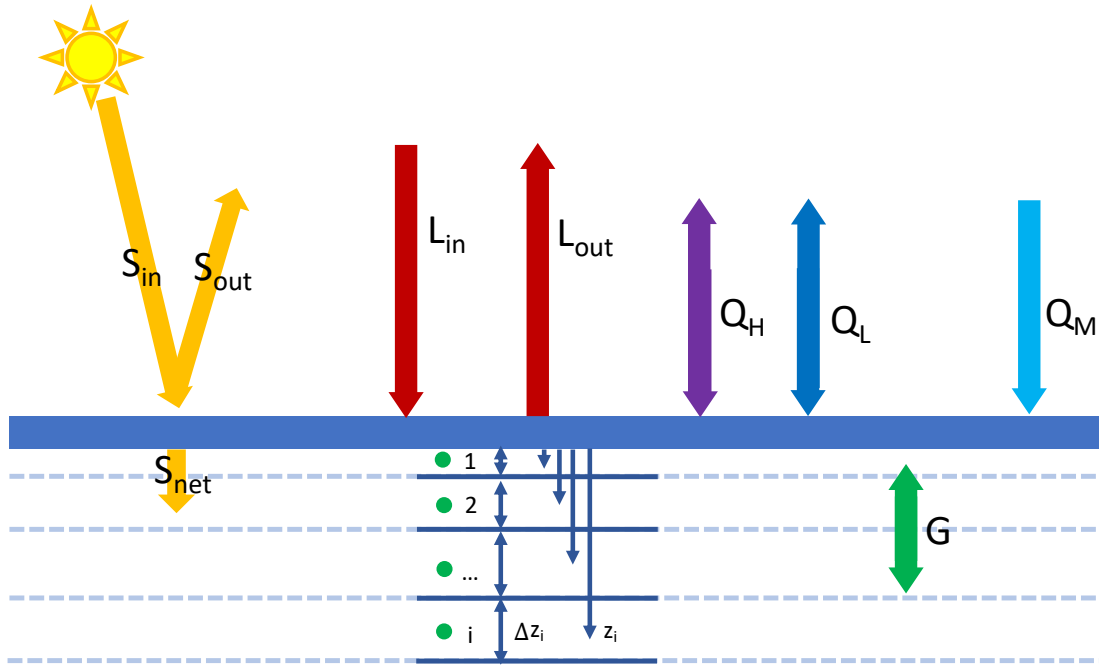


Figure 2: An illustration of the energy balance. The energy fluxes S_{in} , S_{out} , L_{in} , L_{out} , Q_H , Q_L , G and Q_M are represented by arrows. The thick dark blue line represents the glacier surface. The dashed light blue lines represent the upper glacier layers. Each layer has a depth z_i and a thickness Δz_i .

$S_{net} = S_{in} - S_{out} = (1 - \alpha)S_{in}$ and always directed towards the surface.

Just like the Sun, other objects with a nonzero temperature radiate energy. An idealized body that absorbs all radiation and then emits all of it is called a black body. The wavelength of blackbody radiation follows a certain curve, depending on the temperature. The Earth can be approximated as a blackbody in the infrared part of the electromagnetic spectrum, where it radiates most of its energy. L_{out} , the outgoing longwave radiation, is the blackbody radiation of the glacier. The average wavelength of this radiation is much longer than the solar radiation wavelength.

The incoming longwave radiation L_{in} is the radiation from the atmosphere. The atmosphere, however, can not be approximated as a blackbody, since it doesn't absorb and emit all radiation. To calculate it, the blackbody radiation has to be adjusted with the atmospheric emissivity. Emissivity depends on conditions of the atmosphere, most importantly cloud cover. The emissivity of a cloudy atmosphere is higher than that of a clear atmosphere. Due to the low average emissivity of the atmosphere, L_{in} is smaller than L_{out} most of the time. Hence, the net longwave flux is usually directed from the glacier surface towards the atmosphere.

Q_H and Q_L are the sensible and latent heat flux, also called turbulent fluxes. The sensible heat flux is the exchange of heat between the air and the surface due to their temperature difference. The latent heat flux is the energy that is released due to water exchange between the air and glacier surface. It is directed towards the surface (positive) when water condensates or desublimates on the glacier, and negative when water from the surface evaporates or sublimates from the glacier surface. Both turbulent heat fluxes depend on the magnitude of the wind above the surface [7].

The sum of all surface radiation and heat fluxes F determines what happens in the glacier. The energy balance can be written as follows:

$$F = G + Q_M \quad (3)$$

Here, G is the glacier heat flux, describing the flow of heat inside the glacier. Q_M is the flux of energy available for melting. When the glacier surface is at the melting point and F is positive, the incoming energy melts the upper glacier layer. When the temperature is below the melting point, the heat will be transferred into the glacier, which increases the englacial temperature. If there is water inside the snowpack, it (re)freezes at temperatures below 0 °C, also resulting in a temperature increase. If F is negative, the glacier surface loses energy to its surroundings and cools down as a result.

2.2 The Morteratsch glacier

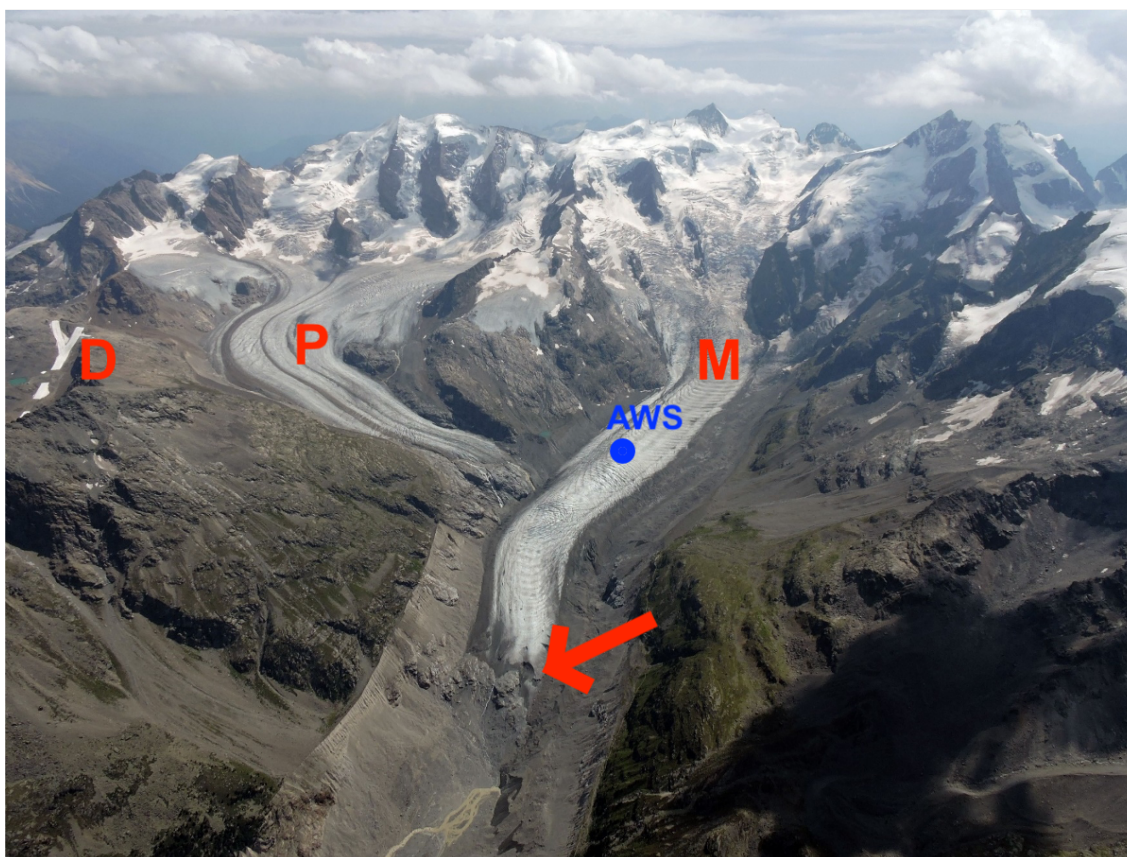


Figure 3: The Morteratsch glacier ('M') and the Pers glacier ('P'). The approximate location of the Automatic weather station is denoted with a blue dot next to 'AWS'. To the left of Pers glacier lies the much smaller Diavolezza glacier ('D'). The arrow points to a bump in the topography. Photo made in August 2017 by C. Levy, Academia Engiadina.

Vadret da Morteratsch is located in the Alps in the south east of Switzerland, near the town Sankt Moritz. It lies in between steep mountains, of which the highest peak is Piz Bernina (4049 m). The Morteratsch glacier ranges in altitude from around 2125 m to 4015 m and is currently 5.8

km long. It has an area of 6.5 km^2 [9]. In Fig. 3, the Morteratsch glacier and its surroundings are shown. Next to the Morteratsch glacier lies a glacier of around equal size, called Vadret da Pers. For a long time, the Morteratsch and Pers glacier were a coupled system: the tongue of the Pers glacier merged with the tongue of the Morteratsch glacier at an altitude of 2400 m. However, in 2012 the glaciers decoupled as a result of the retreat of the Pers glacier. Fig. 3 is taken five years after the decoupling.

To the east of the Pers glacier lies a much smaller glacier, called Diavolezza. Until recently, this glacier was also quickly retreating. This was especially concerning for the ski industry, as the Diavolezza glacier prevents the ski run next to it from becoming too steep [10]. The Diavolezza glacier has been protected against melt in summer by a white fleece for around 15 years. Every year after the accumulation season ends, the fleece is put on the glacier, as can be seen in Fig. 4(a). At the end of the summer, the fleece is removed again. This method seems to have worked, because Diavolezza has since become ten meters thicker [10].

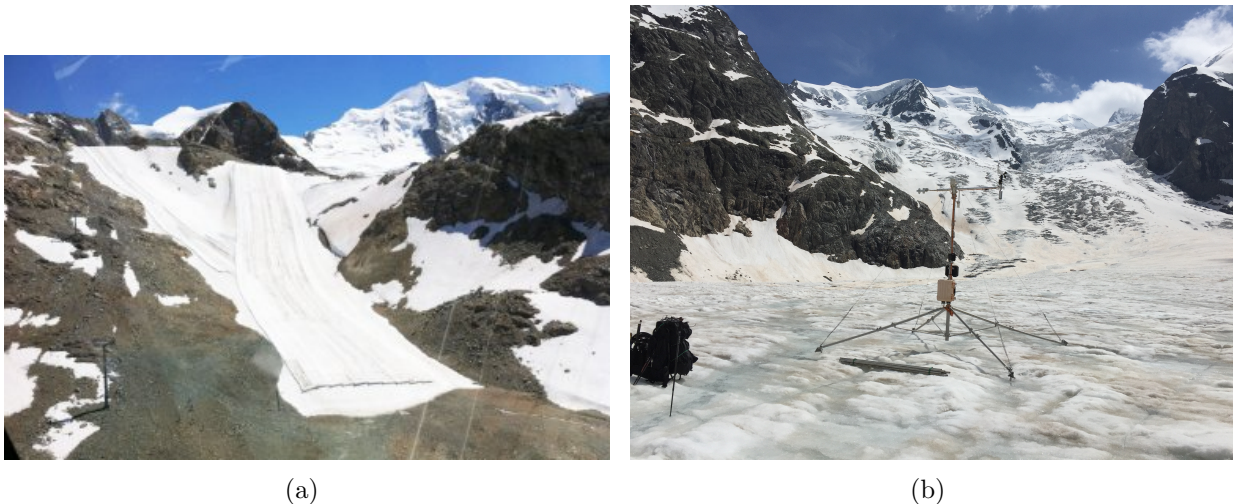


Figure 4: (a) The Diavolezza glacier covered by a fleece. Picture made in September 2016 by J. Oerlemans. (b) The Automatic Weather Station on Morteratsch glacier. Picture taken by F. Keller.

2.2.1 Observations at the Morteratsch glacier

In Fig. 5(a), the length change of the Morteratsch glacier since 1878 is shown [3]. The glacier length has decreased in most years, and the decrease in the last 20 years has been even faster. The decrease is especially significant in 2015 and 2016. This can be explained by the fact that the glacier then retreated over a bump in the topography, indicated by the arrow in Fig. 3.

Since 1995, the Institute for Marine and Atmospheric research Utrecht (IMAU) has been keeping track of conditions at the Morteratsch glacier with an Automatic Weather Station [7]. The Automatic Weather Station (AWS), which can be seen in Fig. 4(b), is an installation standing on the glacier ice. Every half hour, the AWS measures temperature, relative humidity, pressure, ice melt, snow depth, incoming shortwave radiation, outgoing shortwave radiation, incoming longwave

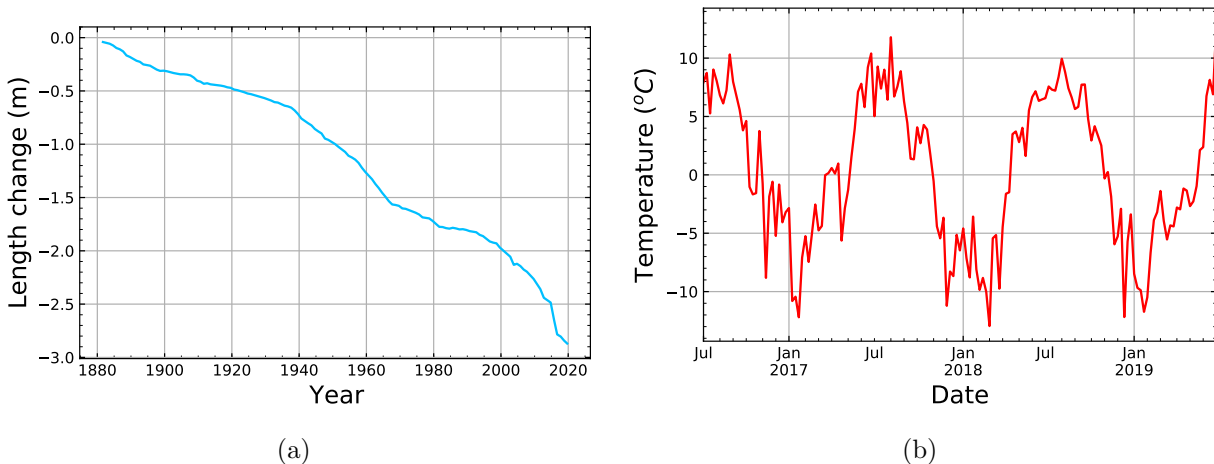


Figure 5: (a) Length change of Morteratsch glacier with respect to 1882. Data from GLAMOS [3]. (b) Weekly average atmospheric temperature measured at the Automatic Weather Station located at 2440 m altitude.

radiation and outgoing longwave radiation. The data is stored locally. Due to the movement and retreat of the glacier, the AWS had to be moved in 2007 and 2016. Currently, it is located at 2440 m altitude. The approximate location of the AWS is indicated in Fig. 3.

In Fig. 5(b), atmospheric temperature as measured by the AWS is shown. The yearly temperature variations are large, ranging from around $-10\text{ }^{\circ}\text{C}$ to $+10\text{ }^{\circ}\text{C}$. The measured wind speed at the AWS is high, on average 2.5 m/s. The direction of the wind is downglacier almost all of the time. This descending wind is called the glacier wind, and it is forced by cold air descending over the mountain slope. The wind increases in magnitude when the temperature difference between the glacier surface and atmosphere is large [7].

Data from the AWS is valuable in research about the Morteratsch glacier because it provides long time series of the measured variables. There are several studies published on these data [6][11]. In a study by Oerlemans and Klok (2004) very relevant to the presented research, AWS data was used to calculate the effect of a heavy summer snowfall in 2000 on the specific mass balance of the Morteratsch glacier [5]. In Fig. 6(a), the surface height as measured by two sonic rangiers is shown. The height increases when the snowfall starts at day 192. The snowfall prevents ice melt for a few days. From the gathered data, Oerlemans and Klok calculated that 224 mm water equivalent (kg m^{-2}) of snow was added to the glacier during the snowfall. In addition, the high snow albedo reduced the ablation by 160 mm water equivalent. The fraction of the total effect relative to the direct effect on the mass balance varied greatly over the glacier, with the highest values on the glacier tongue. It is estimated that this snowfall event could compensate the effect of a $+0.5\text{ K}$ higher mean summer temperature [5].

In another study by Klok and Oerlemans (2002) about a 2D energy and mass balance model of the Morteratsch and Pers glacier, AWS data was used in a different way. The input data of the model came from synoptic weather stations near the Morteratsch glacier, and the AWS data was used to tune the model. [12]. The model used in this research is based on the model by Klok and Oerlemans.

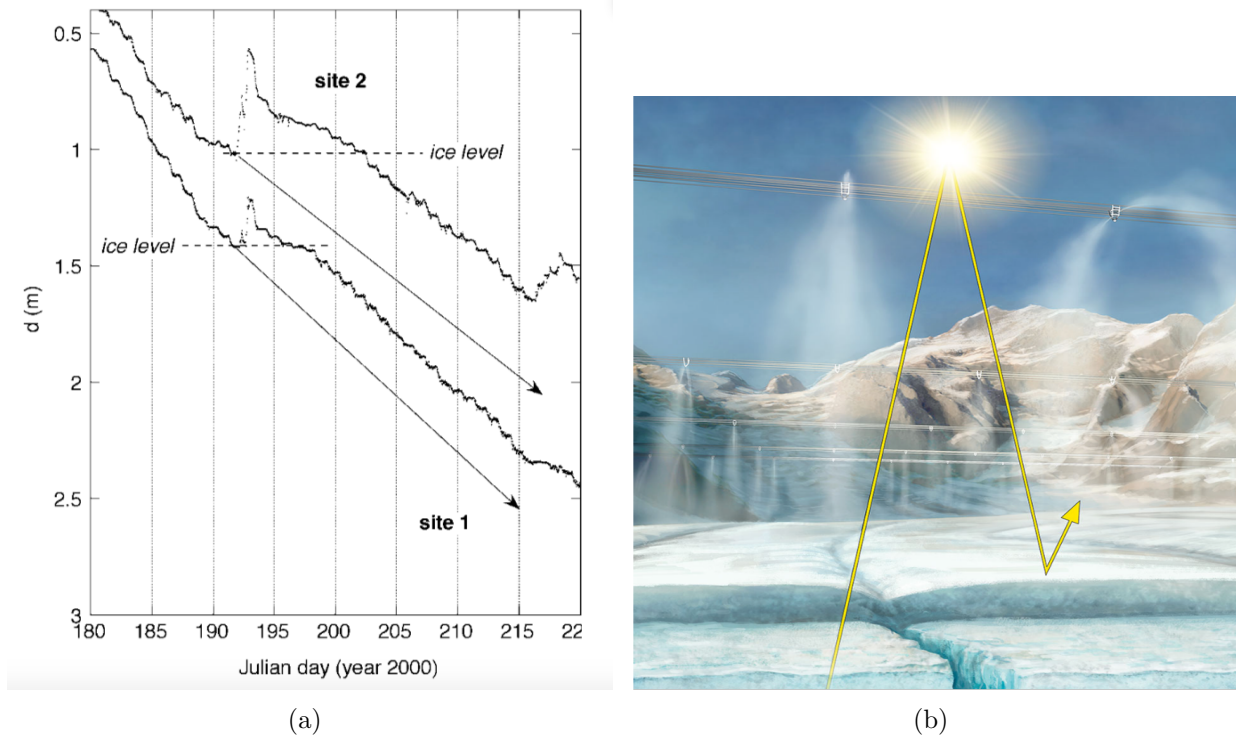


Figure 6: (a) Distance measured from sonic rangers to the glacier surface at 2100 m (site 1) and 2640 m (site 2) in the year 2000. Figure from Oerlemans and Klok 2004 [5]. (b) An impression of the snow shower cable system. Graphic by Andy Pfenninger [13].

2.3 MortAlive project

MortAlive is the project of dr. Felix Keller and prof. dr. Hans Oerlemans to prevent the retreat of the Morteratsch glacier. They were inspired by the success story of the Diavolezza glacier, that had gained mass after it was covered with a fleece during ablation seasons. Because the Morteratsch glacier is much greater in scale, covering it with a fleece is not feasible [4]. Instead, Oerlemans and Keller intend to save the glacier with artificial snow made from meltwater.

The artificial snow can be deposited to the glacier surface by a constellation of snow showers attached to cables that are spanned between the mountain sides. Snow showers are similar to snow lances, long poles that produce artificial snow that are sometimes used in the ski industry. This setup with snow showers on cables is a new technology, of which an impression can be seen in Fig. 6(b). The snow shower that will be used is a Nussy Zero-E, which requires no electrical energy and can produce snow under sufficiently cold conditions [13]. The snow showers create snow by using pressurized air and water to make ice crystals, over which water droplets are sprayed to make the snow [14]. The aim is to use melt water from the Pers glacier for the artificial snow production. It is predicted that a meltwater lake will form next to the Pers glacier in the future. The water will be transported to the Morteratsch glacier by pipes. The position of the future lake with respect to the Morteratsch glacier is shown in Fig. 7.

Not every part of the Morteratsch glacier is suitable for artificial snowfall. First of all, snow cover has a larger effect on the glacier below the snowline, since the amount of ablation there is high and the albedo is relatively low. Secondly, there are constraints for the placement of snow

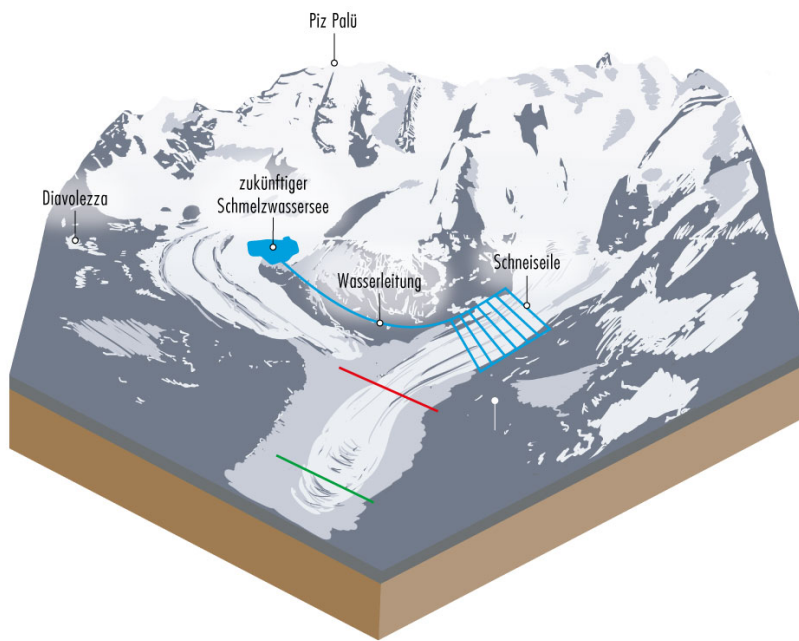


Figure 7: An illustration of the intended setup of the MortAlive project. Picture from MortAlive [13].

showers. The area has to be enclosed by mountains that are steep enough so that the distance between them is not too long. Additionally, it is desirable that the place of supply is not too far away and less than 200m higher than the water source, otherwise additional energy is needed to transport the water. The third constraint is the amount of water available for snow production. Likely, around one quarter of the meltwater of the Pers glacier can be used, especially when a lake forms in the future. Another possible water source is a meltwater lake next to Morteratsch glacier, but that lake contains relatively little water.

Currently, the area around the AWS is favoured as the artificial snow area, as it meets these constraints more or less. As visible in Fig. 7, this area is around the same altitude as the future meltwater lake.

In 2017, a study was done into the feasibility of the plan. A glacier flow model was used to study the impact of keeping the area indicated in Fig. 7 permanently covered with snow. The model predicts that when the goals of the Paris Climate Agreement are met and no artificial snow is supplied, glacier length would decrease significantly: from 5.5 km in 2019 to 3.9 km in 2100. When snow supply starts in 2019 and continues for the rest of the century, the retreat is slowed down, resulting in a glacier length of 4.7 km in 2100 [4].

In my research, I will focus on the impact that artificial snow has on the mass balance of the Morteratsch glacier. First, I will research the effect on the whole glacier, to discover how the currently favoured area compares to other places. Then, I will focus on the mass balance effects in the favoured area. I also aim to find how the mass balance effects are influenced by meltwater availability constraints. Finally, I will look what the sensitivities are with respect to the climate and artificial snow supply.

3 Modelling the Morteratsch glacier

To answer the research questions, I made use of a hypsometric energy balance model of the Morteratsch glacier. In the model, the glacier is divided into 39 elevation bands of 50 m with their respective areas. The hypsometry is shown in Fig. 8. For each height band, the mass and energy balance are calculated.

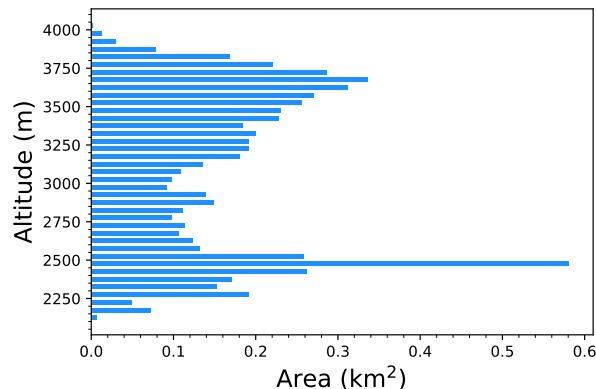


Figure 8: The hypsometry of Morteratsch glacier: the area per height band [9].

Most of the model input data comes from the weather stations Corvatsch and Samedan. The input data is used to determine the snow accumulation, simulate the upper snow and ice layers and calculate the different energy fluxes. From the sum of the surface fluxes (Eq. 2) the glacier heat flux and melt energy are determined. The mass balance at each height band is calculated from the modelled accumulation and ablation.

The model was made in Python by dr. Carleen Tijn-Reijmer and adjusted by me. It is based on an earlier model by dr. Lisette Klok and prof. dr. Johannes Oerlemans [12]. The most important difference between our model and the model by Klok and Oerlemans is that our model is hypsometric instead of 2D. As a consequence, our model is faster, but less precise. In the following sections, I will describe how the model works. Unless stated otherwise, our model follows the model by Klok and Oerlemans as described in the article "Model study of the spatial distribution of the energy and mass balance of Morteratschgletscher, Switzerland" [12].

3.1 Input & evaluation data

The model uses most of its input data from two nearby weather stations. One of them is located in Samedan, a town in a valley 13 km to the north of Vadret da Morteratsch. The other is located at the mountain top Corvatsch 9 km to the west of the Morteratsch glacier. The approximate locations of the weather stations are shown in Fig. 9. The difference between weather conditions measured at Corvatsch and Samedan is large. In the valley where Samedan is located, daily temperature fluctuations are much higher than those at Corvatsch. This is visible in Fig. 10, where the temperatures measured at Samedan and Corvatsch in September 2017 are shown. In winter, temperatures are relatively low in Samedan, due to the 'cold pool' effect: cold air is trapped in the valley [7].

Besides temperature, pressure, incoming shortwave radiation and relative humidity are measured

every hour in Corvatsch and Samedan. Cloud cover is only measured in Samedan. Precipitation is measured at two other weather stations, Bernina-Curtinatsch and Pontresina.

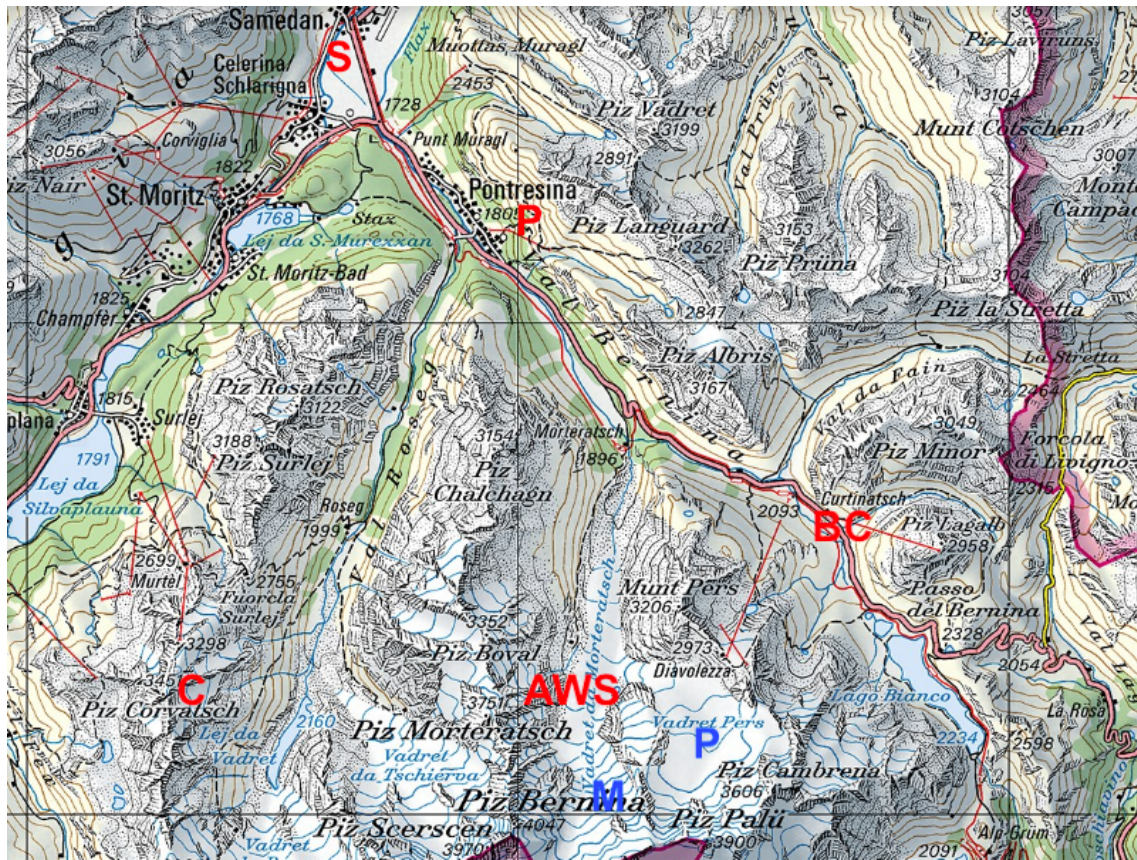


Figure 9: A topographic map of Morteratsch glacier and its surroundings. Morteratsch and Pers glacier are denoted with the blue letters 'M' and 'P'. The weather stations Samedan, Corvatsch, Pontresina and Bernina-Curtinatsch are denoted by *S*, *C*, *P* and *BC*, respectively. Map retrieved from the Schweizerische Eidgenossenschaft[15].

The model is evaluated with data from the Automatic Weather Station (AWS) at the glacier itself, earlier shown in Fig. 4(b). The AWS has been at its current position since June 2016, giving a time series of over 3 years. During the time the model runs, the average position of the AWS was around 2440 m altitude. The AWS measurements can be used to check the model output at the same altitude. Some parameters in the model can be tuned, so that the model becomes more accurate. This involves adjusting the parameter values while evaluating the difference between the model output and measurements. The model tuning process is described in Section 4.1.

In table 1, the input and evaluation data are shown. Pressure in the model is obtained by a linear interpolation with height of the measurements at Samedan and Corvatsch. The mean precipitation measured at Bernina-Curtinatsch and Pontresina is adjusted for height using a precipitation gradient γ_p . Cloud cover is taken directly from the measurements in Samedan. In the first version of the model, relative humidity was linearly interpolated between Samedan and Corvatsch, but this was later changed to an interpolation between the AWS and Corvatsch. Relative humidity represents water vapour concentration relative to the maximum humidity at a

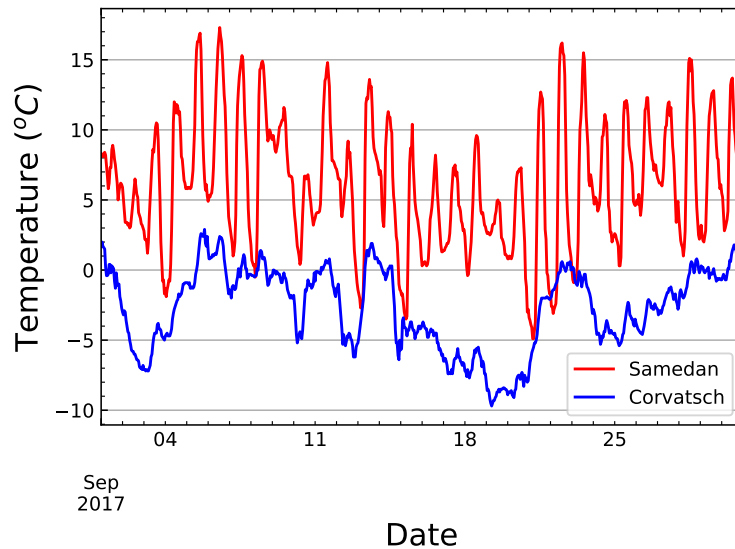


Figure 10: Temperature in September 2017 measured every hour at the weather stations Corvatsch (blue line) and Samedan (red line).

certain temperature. The temperature interpolation was changed from linear to a more complex interpolation using different weights for Samedan and Corvatsch, a constant lapse rate and a constant offset. More details on the relative humidity and temperature interpolations are given in Section 4.1.

3.2 Simulating the snowpack

To be able to simulate energy fluxes from and towards the glacier, it is important to know the characteristics of the upper glacier layers.

The the upper layers of the glacier are simulated so that the englacial temperature and heat flux can be estimated. The upper ten meters are divided into five layers, as illustrated in Fig. 2. The layers increase in thickness Δz with depth. The average layer depths z are at 0.05, 0.20, 0.65, 2.5 and 7.0 meters below the surface. Only the first ten meters of depth are modelled, because the temperature fluctuations below that are small. The modelling of the upper layers is similar as in Klok and Oerlemans (2002), except that five layers are modelled instead of two.

3.2.1 Snowfall

The model keeps track of the amount of precipitation that falls in each elevation band. When the atmospheric temperature T is below 1.5 °C the precipitation is registered as snow, otherwise it falls as rain. The model keeps track of the snow depth by adjusting the snowpack thickness d each time step snow falls or melts away.

In the model, artificial snow deposition can be turned on and off. When the artificial snow setting is turned on, the model checks whether the conditions for artificial snow supply are met

Table 1: Data used for model input and evaluation

	Data	Source
Input	Temperature	Samedan & Corvatsch
	Relative humidity	AWS & Corvatsch
	Pressure	Samedan & Corvatsch
	Cloud cover	Samedan
	Incoming shortwave radiation	Corvatsch
	Precipitation	Pontresina & Bernina-Curtinatsch
Evaluation	Temperature	AWS
	Pressure	AWS
	Ice melt	AWS
	Snow depth	AWS
	Incoming shortwave radiation	AWS
	Outgoing shortwave radiation	AWS
	Incoming longwave radiation	AWS
	Outgoing longwave radiation	AWS

at every time step. The relevant quantity for artificial snowfall is the wet bulb temperature T_{wb} : the temperature an air parcel would be if it was fully saturated with water vapour. When the wet bulb temperature is below $-2\text{ }^{\circ}\text{C}$, artificial snow can be produced.

The wet bulb temperature is calculated in the model from [16]:

$$T_{wb} = T - \frac{e_{sat}(T)(1 - RH)}{\frac{c_p p}{0.622 L_v} + \frac{\partial e_{sat}}{\partial T}} \quad (4)$$

Here, T is the modelled atmospheric temperature in K. From T , the water vapour saturation pressure e_{sat} [hPa] and its derivative $\frac{\partial e_{sat}}{\partial T}$ [hPa/K] can be calculated. RH (fractional) and p [hPa] are the modelled relative humidity and pressure. c_p is the specific heat at constant pressure ($1004\text{ J kg}^{-1}\text{ K}^{-1}$) and L_v the latent heat of vaporization ($2.501 \cdot 10^6\text{ J kg}^{-1}$).

When the wet bulb criterion $T_{wb} < -2^{\circ}\text{C}$ is met, artificial snow is added to the snowpack at a rate of 1.2 mmwe/h . This rate is estimated from the assumption that one snow shower can produce 3000 kg of snow per hour, which is used to cover an area of 2500 m^2 . Additionally, it is assumed that the snow spreads evenly and all snow ends up on the glacier.

3.2.2 Snow density

The model uses the snow depth to determine which of the upper layers consist of snow and which consist of ice. The density ρ_i of each layer $i \in [0,4]$ is calculated in the following way:

$$\rho_i = f_{ice,i} \rho_{ice} + f_{snow,i} \rho_{snow} \quad (5)$$

$$\rho_{snow,i} = \rho_{ice} + (\rho_{freshsnow} - \rho_{ice}) e^{-z_i/10} \quad (6)$$

Here, f_{snow} and f_{ice} are the fractions of snow and ice in a layer. All layers consist only of snow or ice, except the one with the transition from snow to ice. ρ_{ice} and $\rho_{freshsnow}$ are the constant

densities of ice and fresh snow with values of 900 and 350 kg/m³, respectively. The density of snow depends on the average layer depth z_i . The density decays exponentially from the ice density to the fresh snow density with decreasing depth. The density profile is kept constant, so no densification is included.

3.2.3 Glacier heat flux

The energy balance determines what happens to the glacier. When the surface energy flux F (Eq. 2) is positive and the upper layer of the glacier is at the melting point, the incoming energy flux results in melt of the upper layer. If the glacier is below the melting point, the absorption of energy causes the englacial temperature to increase. Similarly, a negative energy surface flux will result in a temperature decrease. Following Klok and Oerlemans, the temperature change in the upper glacier layer is calculated as:

$$\Delta T_0 = \frac{\Delta t}{\rho_0 c_{P0} \Delta z_0} (k_0 \frac{dT_0}{dz} + F) \quad (7)$$

Here, Δt is the model time step (3600 s), ρ_0 [kg/m³] the density and Δz_0 [m] the layer depth, all for the upper layer. c_{P0} [J/kgK] the heat capacity of ice, calculated from T_0 . k_0 [W/mK] is the layer weighted thermal conductivity, calculated from the layer density. The temperature gradient dT_0/dz is estimated from the values at the layer boundaries.

The temperature change for every other layer $i \in [1,4]$ is calculated as:

$$\Delta T_i = \frac{\Delta t}{\rho_i c_{Pi} \Delta z_i} (k_i \frac{dT_i}{dz} - k_{i-1} \frac{dT_{i-1}}{dz}) \quad (8)$$

The temperature at 10 meters depth T_{10m} is fixed. For all height bands below the ELA (2982 m), T_{10m} is at the melting point. For the height bands above that, T_{10m} decreases with 0.1 K every 50 meters.

3.2.4 Water percolation

Water originating from rain or glacial melt can percolate into the snowpack. In addition to Klok and Oerlemans, the effect of refreezing water on the mass and energy balance is taken into account.

The maximum amount of water that can refreeze in a layer is given by W_{max} [mm w.e.] = $\rho_{water} \Delta z_i (\rho_{ice} - \rho_i) / \rho_{ice}$. As water freezes, latent heat is released. This energy results in a temperature increase in snow temperature equal to:

$$\Delta T_i = \frac{W_{fr,i} L_m}{\rho_i c_{Pi} \Delta z_i} \quad (9)$$

Here, $W_{fr,i}$ [mm w.e.] is the amount of water that freezes in a layer and L_m is the latent heat of melting ($3.34 \cdot 10^5$ J/kg). The refreezing continues until all available water is refrozen or until the temperature reaches 0 °C.

After each time step, all water that is left percolates to the next layer, except the water held by capillary forces against gravity.

3.3 Surface energy fluxes

3.3.1 Incoming shortwave radiation

To determine the incoming shortwave radiation at each elevation band, the solar radiation at the top of the atmosphere is adjusted for the inclination of the sun with respect to the surface and interference with the atmosphere.

Following Klok and Oerlemans, incoming shortwave radiation at the glacier is calculated as follows:

$$S_{in} = T_{trans}T_{cloud} \cos(Z)S_{TOA} \quad (10)$$

Here, the shortwave radiation at the top of the atmosphere S_{TOA} is all the solar radiation that reaches a surface oriented to the sun, without atmospheric interference. S_{TOA} varies a bit over the year with the distance to the sun.

The zenith angle Z is the angle between the vertical of the earth surface and the position of the sun, as illustrated in 11. It depends on the daily and seasonal cycle of incoming solar radiation and is calculated from the latitude, declination and time of the day.

T_{Trans} represents the fraction of solar radiation that is transmitted through the atmosphere limited by Rayleigh scattering, gas absorption and scattering by water vapour and aerosols. It is calculated for every height band of the Morteratsch glacier, since it depends on height through the thickness of the atmosphere. The factor T_{cloud} is the transmission of solar radiation through clouds. T_{cloud} is determined as a constant for the whole glacier with Eq. 10 using T_{trans} and measurements of S_{in} at Corvatsch.

When incoming shortwave radiation is calculated using equation 10, important factors like the slope, orientation and shading at the glacier are excluded. Klok and Oerlemans took these factors into account by using a Digital Elevation Model. Since this model is not 2D, topography effects are modelled differently.

Slope and orientation of the glacier surface were determined from the characteristics of the flowline used in the glacier flow model of the Morteratsch glacier by Oerlemans in 2017 [4]. That model started at 3700 m. Slope and orientation for higher altitudes were estimated from the topographical maps of the Switzerland Confederation [15].

The effect of surrounding topography is taken into account by introducing the angle describing the topography height H_{topo} . This angle represents the part of the sky that is obstructed by the topography, and is illustrated in Fig. 11. In the model, for each elevation band the average H_{topo} over all directions is used as input. The value of H_{topo} is difficult to obtain. It was estimated by finding the maximum possible topography angle $H_{topo,max}$ at each height band using the topographic map [15]. The average topography angle was assumed to be a constant fraction f_{topo} of this angle, so that it is given by $H_{topo} = f_{topo}H_{topo,max}$. The fraction f_{topo} was estimated from observations at the AWS.

If the shading, orientation and slope of the glacier are taken into account, the direct and diffuse fraction of solar radiation have to be calculated separately. The direct solar radiation is calculated as:

$$S_{dir} = f_{dir}T_{trans}T_{cloud}\cos(Z_a)S_{TOA} \quad (11)$$

where f_{dir} is the direct fraction of all solar radiation, calculated from $f_{dir} = 0.2 + 0,65(1 - cc)$ with cc the fractional cloud cover. Z_a is the zenith angle adjusted for the slope and orientation of the

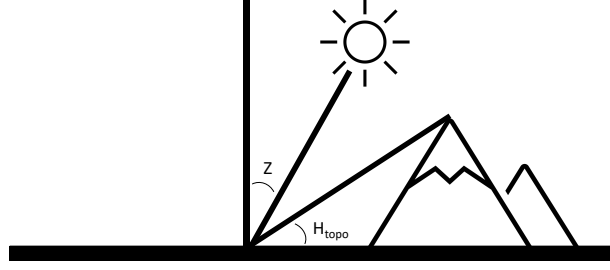


Figure 11: Illustration of the zenith angle Z and the topography angle H_{topo} on a horizontal surface.

glacier surface. There is no direct solar radiation when $Z > 90^\circ - H_{topo}$.

The diffuse solar radiation is given by:

$$S_{dif} = f_{dif} V_f T_{trans} T_{cloud} \cos(Z) S_{TOA} \quad (12)$$

Here, $f_{dif} = 1 - f_{dir}$. Now, Z is the zenith angle for a horizontal surface, as the diffuse radiation comes from the whole sky. Everything has to be multiplied by the view factor V_f because topography obstructs light from a part of the sky. Finally, the new incoming solar radiation is calculated by adding S_{dir} and S_{dif} .

3.3.2 Albedo

When modelling the albedo, it is important to take the varying snow albedo into account. Following Klok and Oerlemans (2002), this is done by tracking the time since the last snowfall, as fresher snow has a higher albedo. The snow albedo is parameterized as follows:

$$\alpha_{snow}(t) = \alpha_{firn} + (\alpha_{freshsnow} - \alpha_{firn}) e^{-\frac{t}{t^*}} \quad (13)$$

Here, t is the time since the last snowfall. The snow albedo is equal to the $\alpha_{freshsnow}$ (0.9) just after snowfall and decays exponentially to α_{firn} (0.53) over time. After a time t^* the snow albedo has lowered to a value of 0.67. After tuning, the time scale t^* was chosen as 13 days. This differs from the value of Klok and Oerlemans, who had $t^* = 21.9$ days [12].

The albedo α is calculated from the snow albedo and the snow depth d with the following equation:

$$\alpha(t, d) = \alpha_{snow}(t) + (\alpha_{ice} - \alpha_{snow}(t)) e^{-\frac{d}{d^*}} \quad (14)$$

If there is no snow, the albedo is equal to α_{ice} (0.3). When more snow accumulates, α increases to α_{snow} . The depth scale d^* was tuned to 2.2 cm. The value used by Klok and Oerlemans was 3.1 cm [12].

The outgoing shortwave radiation is obtained by multiplying the incoming shortwave radiation with the albedo.

3.3.3 Outgoing longwave radiation

The outgoing longwave radiation can be calculated easily because the glacier surface can be treated as a black body. It is given by:

$$L_{out} = \sigma T_0^4 \quad (15)$$

Here $\sigma = 5.67 \cdot 10^{-8} \text{ J s}^{-1} \text{ m}^{-2} \text{ K}^{-4}$ is the Stefan Boltzmann constant and T_0 is the temperature of the upper layer of the glacier. How T_0 changes over time is determined by the heat flux, explained in Section 3.2.3.

3.3.4 Incoming longwave radiation

The incoming longwave radiation is the radiation from the atmosphere. The atmosphere is a grey body, so the blackbody radiation formula has to be adjusted for the emissivity ϵ :

$$L_{in} = \epsilon \sigma T^4 \quad (16)$$

The emissivity depends on the conditions of the sky. Following Klok and Oerlemans (2002), the emissivity is calculated from the cloud emissivity ϵ_{cloud} and clear sky emissivity $\epsilon_{clearsky}$ as:

$$\epsilon = (1 - cc^2)\epsilon_{clearsky} + cc^2\epsilon_{cloud} \quad (17)$$

Here, cc is the fractional cloud cover, which can take values between 0 and 1. The emissivity of clouds is $\epsilon_{cloud} = 0.984$. The emissivity of a clear sky $\epsilon_{clearsky}$ is calculated from:

$$\epsilon_{clearsky} = 0.23 + b\left(\frac{e}{T}\right)^{\frac{1}{8}} \quad (18)$$

Here e is the water vapour pressure in Pa and T the atmospheric temperature in K. b is a constant parameter, chosen as $0.395 \text{ (K/Pa)}^{1/8}$ after tuning. This is different from the value of Klok and Oerlemans, who found a value of $0.433 \text{ (K/Pa)}^{1/8}$ by tuning [12].

3.3.5 Turbulent fluxes

Following Klok and Oerlemans, the sensible heat flux Q_H and latent heat flux Q_L are modelled as:

$$Q_H = \frac{1}{2} \rho c_p (C_{kat} + C_b) (T - T_0) \quad (19)$$

$$Q_L = \frac{\rho R_d L_{s/v}}{2pR_v} (C_{kat} + C_b) (e - e_s(T_0)) \quad (20)$$

Here ρ is the modelled air density. Both formulas depend on C_b and C_{kat} , the base and katabatic exchange coefficients. C_{kat} represents the exchange due to the glacier wind and depends on the temperature difference between the atmosphere and upper glacier layer $T - T_0$. In the formula for Q_L , p [Pa] is the atmospheric pressure, e [Pa] the atmospheric water vapour pressure and e_s [Pa] the saturated water vapour pressure just above the glacier surface. R_d ($287.05 \text{ J kg}^{-1} \text{ K}^{-1}$) and R_v ($461.51 \text{ J kg}^{-1} \text{ K}^{-1}$) are the gas constants of dry air and water vapour. $L_{s/v}$ is the latent heat of sublimation ($2.83 \cdot 10^6 \text{ J/kg}$) when the temperature is below the melting point and of vaporization ($2.50 \cdot 10^6 \text{ J/kg}$) when it is above the melting point.

3.4 Mass balance

For each height band h and time step t , the specific mass balance $B_{h,t}$ is calculated.

$$B_{h,t} = P_{h,t} + M_{h,t} + R_{h,t} + S_{h,t} \quad (21)$$

$$= P_{h,t} + \frac{E_{M,h,t}}{L_m} + R_{h,t} + \frac{Q_{L,h,t}^s \Delta t}{L_s} \quad (22)$$

Here $P_{h,t}$ is the snow precipitation, $E_{M,j,t}$ the melt energy per unit area [J/m^2], $R_{h,t}$ the refreezen water and $Q_{L,h,t}^s$ the latent heat flux for (de)sublimation (Q_L when the temperature is below 0°C).

The total mass balance is obtained by summing the product of the area and specific mass balance over time and all height bands, and divided by the total area to obtain a value per unit area:

$$B = \frac{1}{A} \sum_{\text{height}} \sum_{\text{time}} A_h B_{h,t} \quad (23)$$

4 Evaluating the model

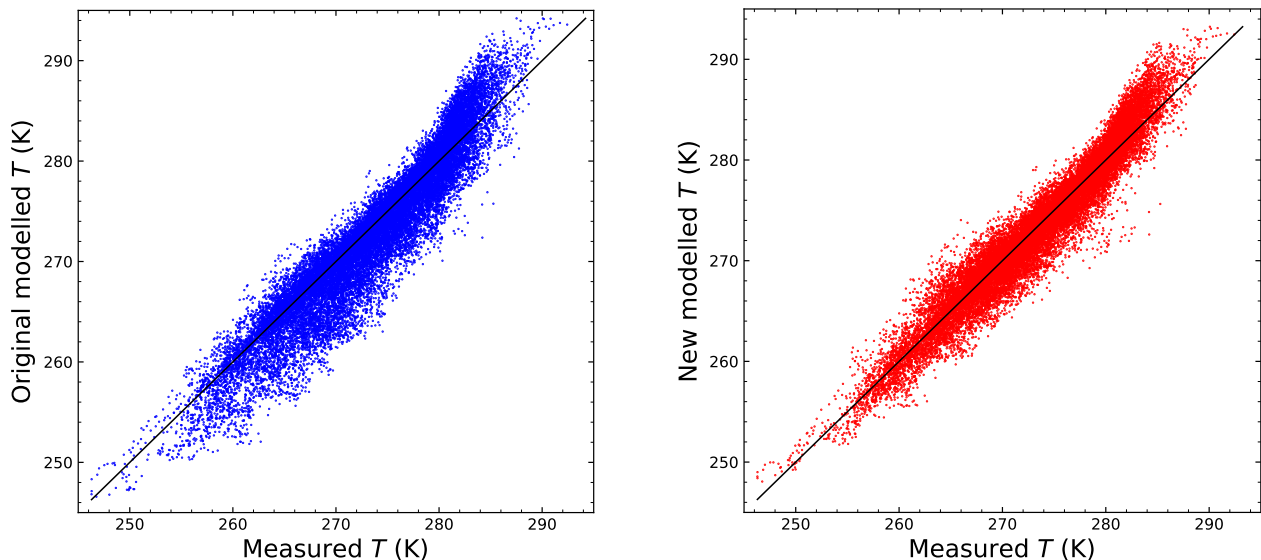
In this section, the model outcomes are compared to measurements at the AWS and the tuning process is described. Then, the outcomes of the reference run are discussed and the results of the sensitivity analysis are evaluated.

4.1 Model tuning

Evaluation data is important for creating an accurate model. In this research, data from the Automatic Weather Station (AWS) was used to compare the model output at the same altitude as the AWS. The data were evaluated from 11/09/2016 to 11/09/2019. On the basis of the comparison between data, some changes were made to the modelling of the temperature, relative humidity, incoming shortwave radiation, incoming longwave radiation and albedo. The modelling of the precipitation was changed based on other observations. In some cases only some parameters were changed, in other cases more explicit changes to the model were made.

4.1.1 Temperature

The model temperature is determined from measurements at Samedan and Corvatsch. Klok and Oerlemans determined the atmospheric temperature by a linear interpolation with height between the measurements at Corvatsch and Samedan. This gives a quite good agreement with the measurements ($R = 0.95$, bias = -0.63 K, RMSE = 2.66 K), as can be seen in Fig. 12(a).



(a) Linear interpolation between Corvatsch and Samedan.

(b) Adjusted weighted average between Corvatsch and Samedan.

Figure 12: Scatter plots of the hourly modelled and measured temperature at 2440 m. Points above the black line are modelled too high, points below the line are modelled too low.

However, linear interpolation might not be the best approach, since the conditions at Samedan and Corvatsch are very different, as was shown earlier in Fig. 10. Therefore, I explored other ways

to model the temperature.

I decided to give more weight to the Corvatsch measurements, since they are more similar to the conditions at the Morteratsch glacier. I did this by taking a weighted average of the temperatures of Corvatsch and Samedan at their midpoint with a constant offset of +1.8 K to correct for the higher weight of Corvatsch. That temperature was then extrapolated to other heights using a constant lapse rate. I choose a lapse rate of -5.5 K based on the average temperature difference between the AWS and Corvatsch. This interpolation can be seen in Fig. 12(b) and turned out to be better ($R = 0.97$, bias = 0.04 K, RMSE = 1.86 K). The variation over the day is smaller and closer to the measurements. Additionally, the bias in midwinter has declined.

4.1.2 Relative humidity

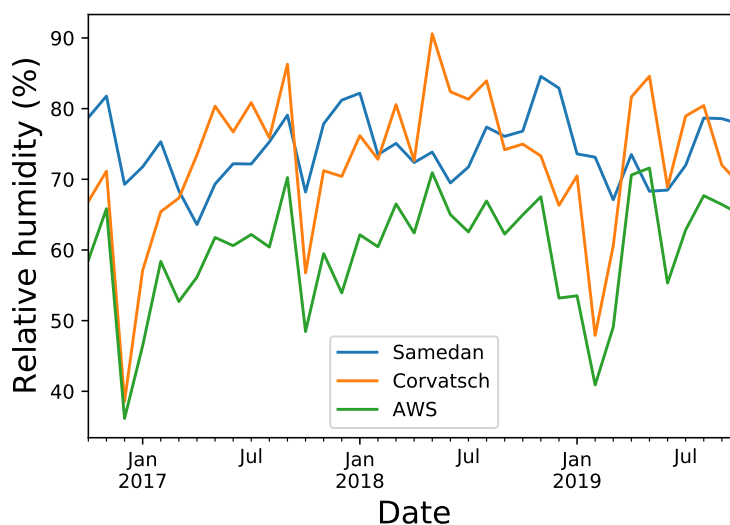


Figure 13: Monthly average relative humidity measured at Corvatsch, Samedan and the Automatic Weather Station at Morteratsch glacier.

Initially, relative humidity (RH) was calculated by linearly interpolating the measurements at Samedan and Corvatsch with height. However, when I compared the modelled relative humidity at 2425 m to the measurements at the same height by the automatic weather station, I noticed that they didn't match well: the correlation was only 0.77, and the measurements were on average 14 % higher. In Fig 13, the monthly average measurements from the AWS, Samedan and Corvatsch are all plotted. From this figure, it becomes clear that the RH measured at the AWS is always lower than at Corvatsch and Samedan. This can be explained by the presence glacier wind at the AWS. Since the air comes from higher colder places, its humidity is low, resulting in a lower relative humidity lower on the glacier. There is a high mountain climate at Corvatsch, which is similar to the climate at the highest glacier altitudes. With this knowledge, linearly interpolating RH measurements from Corvatsch and Samedan doesn't seem ideal. Instead, I choose to linearly interpolate the data from Corvatsch and the AWS. This likely matches better with reality, but unfortunately I cannot check that since the control data for the relative humidity is now used as input.

4.1.3 Precipitation

Precipitation at each altitude is calculated by adjusting the measured precipitation at Bernina-Curtinatsch with a precipitation gradient γ_p . The initial value used by Klok and Oerlemans of γ_p was 0.4 mm w.e./yr/m, based on research in the area of the Morteratsch glacier [17][12]. This means that the yearly precipitation increases with 0.4 mm per meter with increasing altitude. It is difficult to check whether the modelled snow precipitation is correct. It is not ideal to compare the measured and modelled snow depth, since modelled snow depth also depends on the rain-snow temperature cutoff and the density profile.

However, the snow precipitation can be obtained from ice core measurements, as the snow density can be determined from those measurements. From an ice core at the top of the accumulation zone of Pers glacier, a yearly accumulation rate of 2.6 ± 0.8 m w.e./yr was found for 1992-2001 [18][4]. For $\gamma_p = 0.4$ mm w.e./yr/m, the modelled yearly accumulation at the highest elevation band is 1.8 m w.e./yr. Because this is significantly lower than the measured rate, I decided to increase γ_p to 0.6 mm w.e./yr/m. This new rate resulted in 2.2 m w.e./yr modelled accumulation, closer to the measured rate. It should be noted that this decision had to be based on personal judgement of little available information.

4.1.4 Incoming shortwave radiation

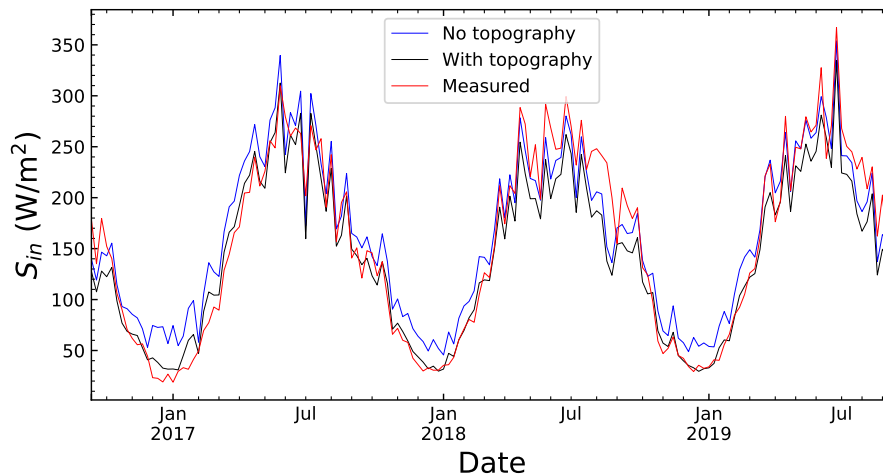


Figure 14: Seven day average incoming shortwave radiation at 2425 m. Measurements by the AWS are represented by the red line. Modelled radiation with topography effects (black line) and without topography effects (blue line) are compared.

First, I evaluated the modelled incoming shortwave radiation when no topography effects were included. The slope and topography angle H_{topo} were equal to zero, and the orientation was towards the north. The results at 2400-2450 m altitude are compared to the measurements at AWS in Fig. 14. As expected, the modelled radiation exceeds the measurements most of the time. The difference is especially large during winters. The blue line in Fig. 15 shows that the incoming solar radiation without topography effects increases with altitude, as the atmosphere gets thinner. When slope and orientation are taken into account, the results change significantly. In Fig. 15, the green line represents this case. It shows a large variation with altitude. Most of this variation

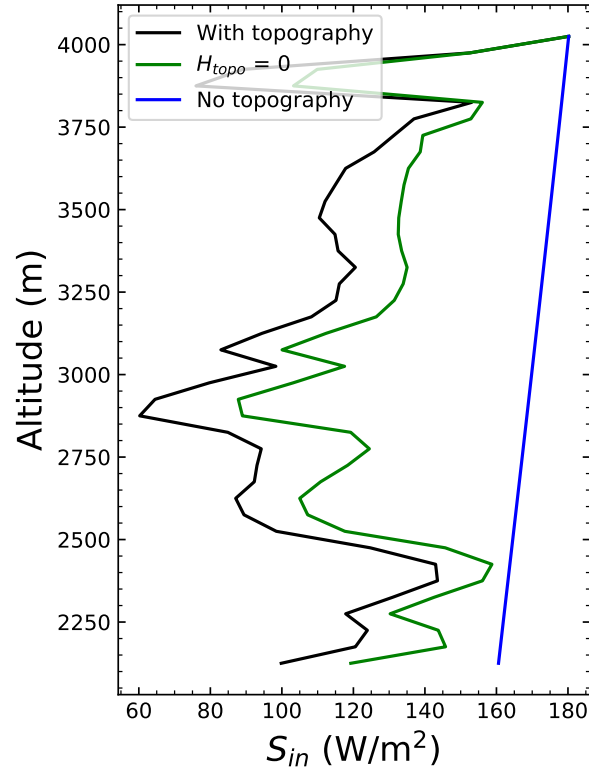


Figure 15: Average modelled incoming shortwave radiation as a function of height. The blue line shows modelled radiation without topography effects. For the green line, slope and azimuth of the surface are taken into account but H_{topo} is neglected. The black line shows the final modelled shortwave radiation with all topography effects.

is due to the slope, as the orientation of the glacier varies little.

To include the effect of shading by the topography as well, the topography angle H_{topo} had to be estimated. This was done by varying the fraction f_{topo} of the measured maximum topography angle $H_{topo,max}$. The results at the AWS height were compared to the AWS measurements. By evaluating the differences, f_{topo} was tuned to 0.7. The results including the tuned topography angle, slope and orientation are shown by the black line in Fig. 14. This modelling matches well with the measurements, especially during winters. H_{topo} is of greater importance during winters because of the on average lower solar elevation. Surprisingly, the measured radiation is much higher during the last two summers. It is not certain what causes this. It is possible that the AWS doesn't stand completely perpendicular to the glacier surface, but a bit more oriented towards the sun. In Fig. 15, the results of including all topography effects are compared to the results of including only slope and orientation of the glacier surface. From this figure, it becomes clear that the effect of shading by topography is generally smaller than that of the glacier slope, but there is large variation over the glacier. At the altitude band of the AWS (2400-2450 m), the effect of H_{topo} is bigger than that of the slope as the slope angle is small.

4.1.5 Incoming longwave radiation

A scatter plot of the initial model output for L_{in} is shown in Fig. 16(a). The daily modelled incoming longwave radiation was on average 8.6 W/m^2 higher than the measured value ($R = 0.92$, bias = 8.6 W/m^2 , RMSE = 20 W/m^2). I varied with the parameters b and ϵ_{cloud} and found that adjusting b was most effective at reducing the bias while maintaining a high correlation. This indicates that the emissivity of a clear sky (Eq. 18) was modelled too high. The result can be seen in Fig. 16(b). By changing b from 0.433 to 0.395, I reduced the bias to 1.5 W/m^2 .

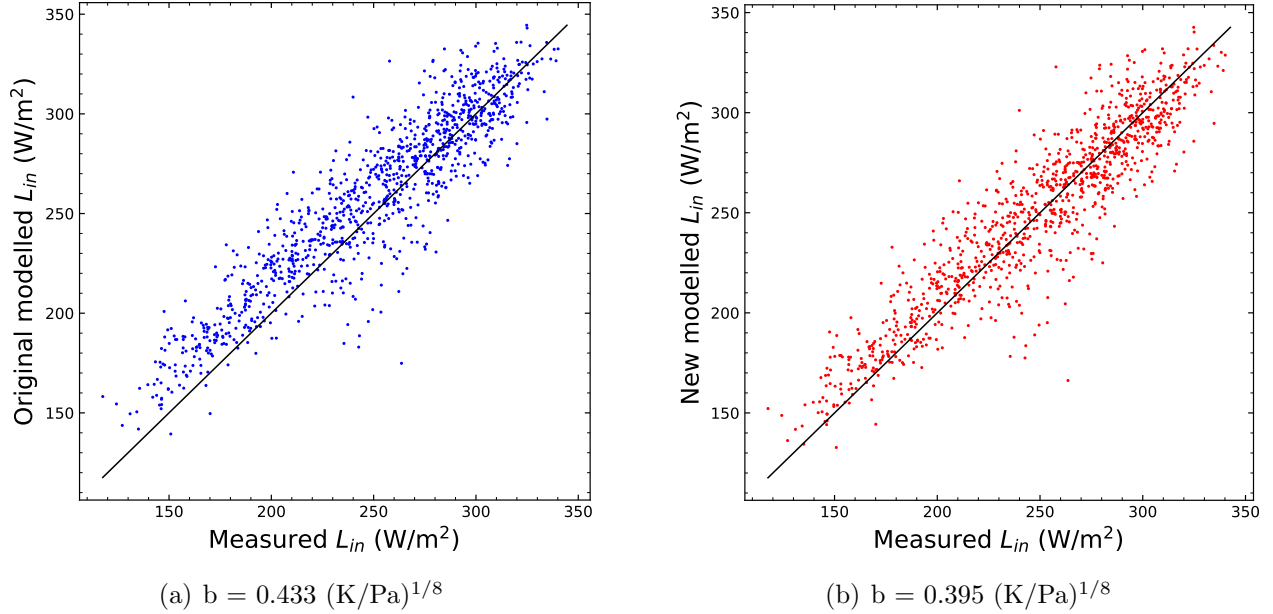


Figure 16: Scatter plots of the daily modelled and measured incoming longwave radiation at 2440 m. Points above the black line are modelled too high, points below the line are modelled too low.

4.1.6 Albedo

Initially, I used the same values for t^* and d^* in the albedo parameterization as Klok and Oerlemans. That resulted in a reasonable agreement with the albedo calculated from the measurements ($R = 0.906$, bias = 0.024 , RMSE = 0.12). The albedo at the end of ablation season was modelled too high. Therefore, t^* was lowered to find a better match. In addition, albedo changes at early snowfall events were often modelled too low. By increasing d^* this was improved. The agreement between the model and measurements improved because of these changes ($R=0.935$, bias = 0.014 , RMSE = 0.096). In Fig. 17, the final result is shown.

From 1995-2007, the AWS was located on a lower position at the glacier tongue. Research from that period indicates that the the albedo was very low at that position due to dust accumulation [6]. To account for this effect, I added a gradient in the modelled ice albedo. Above 2400 m α_{ice} is always equal to 0.3, below that altitude it decreases linearly with height to 0.2 at the lowest point of the glacier.

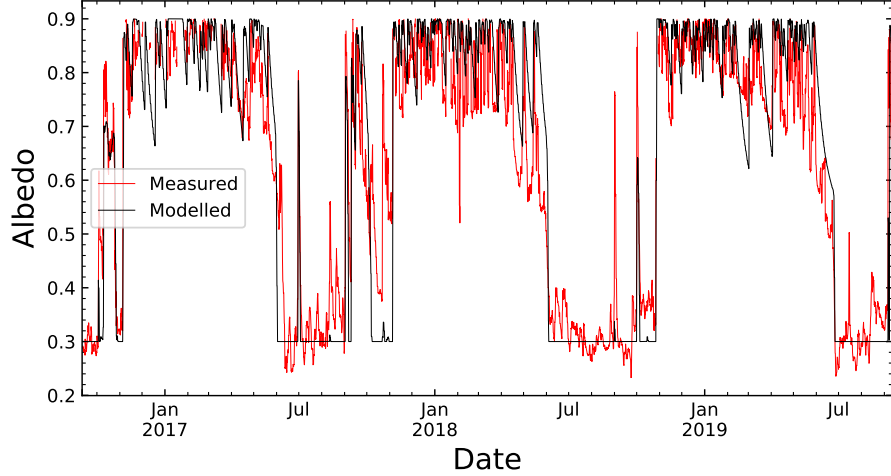


Figure 17: Measured and modelled rolling daily average albedo.

Table 2: Comparison between model and measurements at 2400-2450m. IM (ice melt) is based on 3-day averages, α is based on 24-hour running averages. The fluxes are daily averages. The rest are hourly values.

	period	R	bias	RMSE
p	hourly	0.99	+0.45 hPa	1.17 hPa
T	hourly	0.97	-0.0089 K	1.9 K
d	hourly	0.96	-0.20 m	0.32 m
S_{in}	daily	0.95	-11 W/m ²	35 W/m ²
S_{out}	daily	0.95	-1.9 W/m ²	56 W/m ²
α	running 24-hour	0.93	0.014	0.098
L_{in}	daily	0.93	+1.5 W/m ²	18 W/m ²
L_{out}	daily	0.97	+0.11 W/m ²	7.5 W/m ²
IM	3-daily	0.95	-0.22 mm	22 mm

4.2 Model evaluation

In table 2, the final evaluation between the model outputs and measurements is shown. Here I discuss only the quantities that were not tuned: pressure, S_{out} , L_{out} , ice melt and snow depth. Modelled and measured pressure are compared in Fig. 18(a). The correlation between the modelled and measured pressure is very high ($R = 0.99$) and the bias and root mean square error are low.

Modelled L_{out} matches well with the data, as can be seen in Fig. 18(b). Because the outgoing longwave radiation is calculated with $L_{out} = \sigma T_0^4$, this indicates that the surface temperature was modelled well.

In Fig. 18(d), modelled and measured S_{out} are compared. They correspond well to each other, indicating that combined modelled S_{in} and α are reasonable.

Ice melt (IM) is plotted in Fig. 19 and matches well. Over the three years evaluated, the AWS measures 15.27 m of ice melt. The model is only 8 centimeters off with a modelled 15.19 meter.

The snow depth is plotted in Fig. 20. The modelled values have a high correlation ($R = 0.96$) with the measurements. However, the bias is high: the modelled snow is 0.20 meter lower than

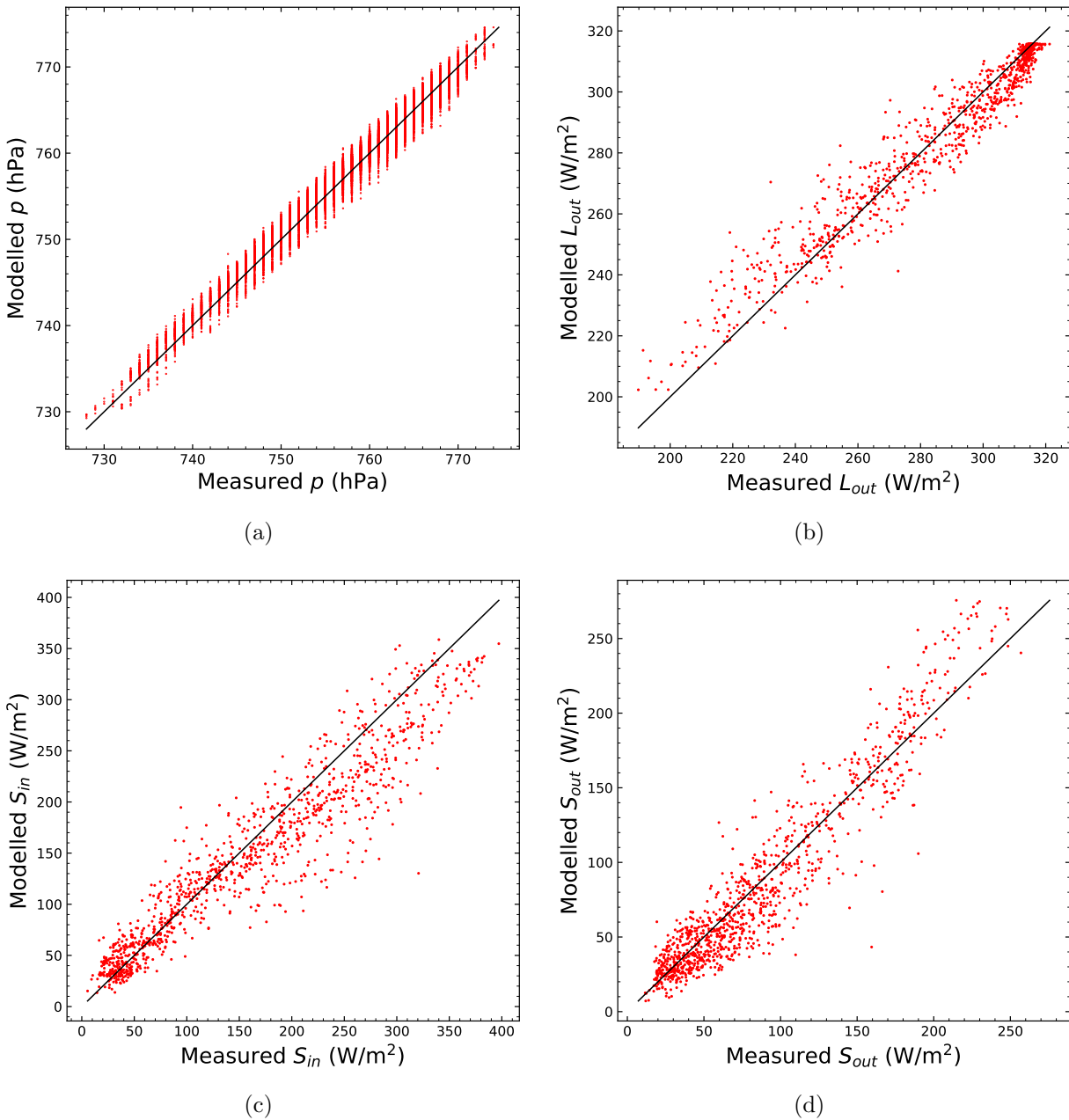


Figure 18: Scatter plots of modelled and measured quantities: (a) hourly pressure; (b) daily outgoing longwave radiation; (c) daily incoming shortwave radiation; and, (d) daily outgoing shortwave radiation.

the measured snow depth. Likely, the discrepancy is due to the fact that the densification of snow is not modelled. This also explains why the snow declines are much steeper in the measured case. Although the modelled snow density is probably not correct. Despite the fact that the snow height is not modelled correctly, the modelled snow mass probably matches better, since that does not depend on the density parameterization. For the albedo modelling, the time when the snowpack has melted away is the most important to model correctly. That timing is likely modelled well, since it depends on the snow mass.

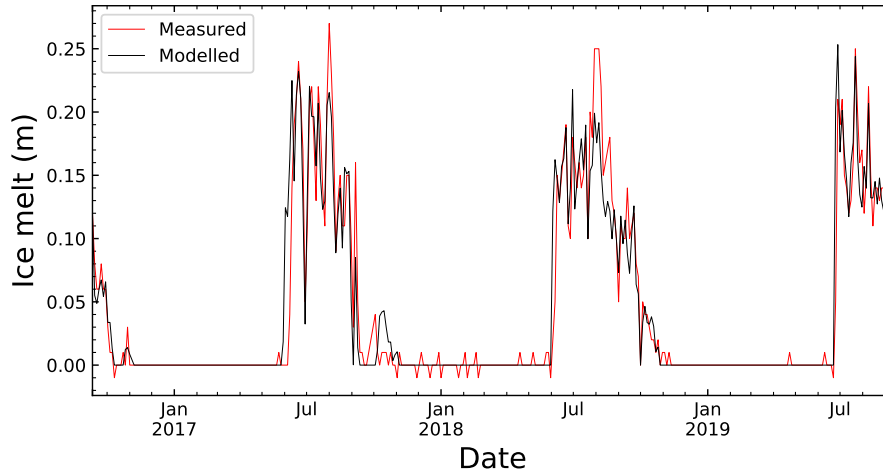


Figure 19: Measured and modelled 3-day average ice melt

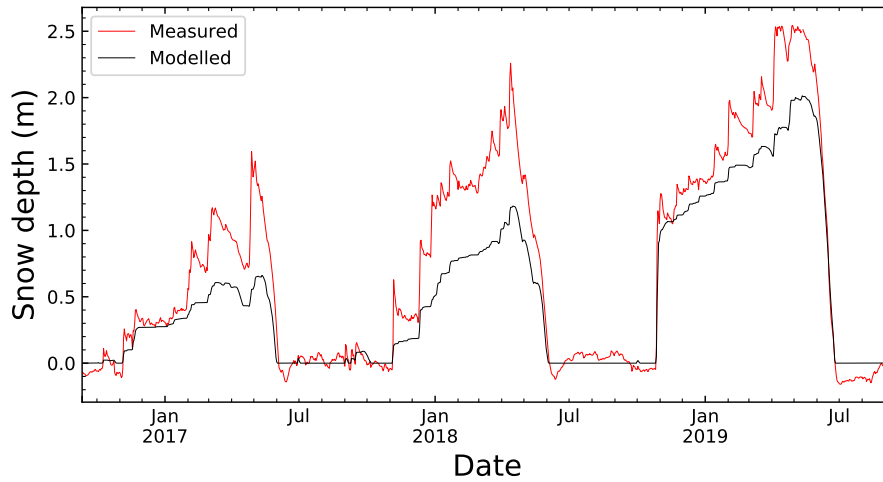


Figure 20: Measured and modelled daily average snow depth.

4.2.1 Comparison with Klok and Oerlemans

Klok and Oerlemans (2002) also evaluated their model with AWS data. They found $R=0.96$ for daily averaged S_{in} [12], comparable to my finding ($R=0.95$). This suggests that my 1D modelling of incoming shortwave radiation with tuning of the topography angle is comparable to their 2D modelling at the AWS altitude. However, for the whole glacier 2D modelling will perform better. For S_{out} , Klok and Oerlemans found a R of 0.89 [12], lower than my finding of $R=0.95$. Since S_{in} performance was similar, this suggests that my albedo modelling was more accurate.

For L_{in} and L_{out} , Klok and Oerlemans find correlations of 0.91 and 0.97, respectively [12], comparable to what I found. Surprisingly, Klok and Oerlemans modelled L_{in} too low (bias = -6.8 W/m^2), whereas I had a bias of $+8.6$ W/m^2 when I modelled it using the same value for b .

4.3 Reference run

In the following sections, the results from the model reference run, i.e. without artificial snow, are discussed. The model results cover the period from the 20th October 2016 to the 20th October

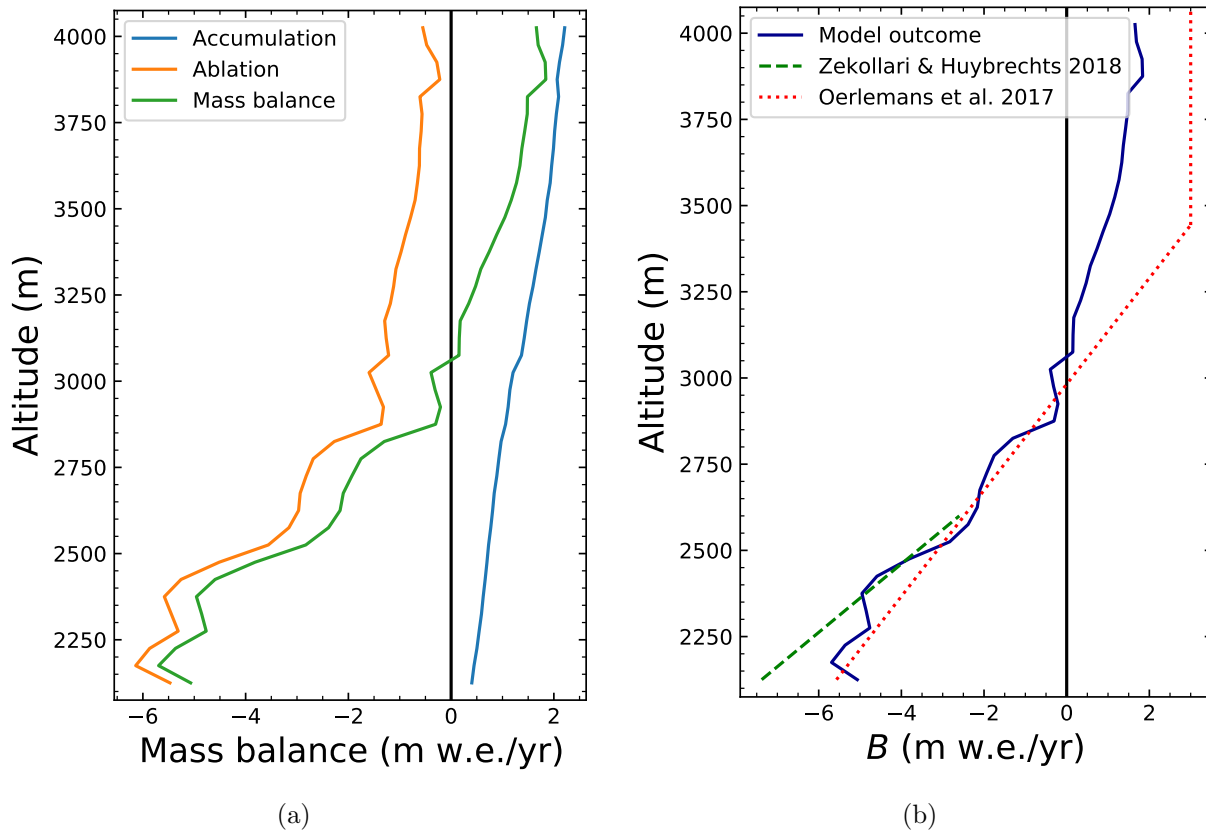


Figure 21: (a) Yearly specific mass balance for the Reference run over the period 20 October 2016 to 20 October 2019. The ablation is shown by the orange line and the accumulation is shown by the blue line. The specific mass balance (green line) is obtained by adding the accumulation and ablation. (b) Yearly modelled specific mass balance (blue line) compared with findings from literature. The green dashed line shows the best linear fit to the stake measurements from 2001-2016 in the ablation zone by Zekollari & Huybrechts [19]. The red dotted line shows the input to the ice flow model by Oerlemans [4].

2019, encompassing three mass balance years.

The yearly average specific mass balance is shown in Fig. 21(a). At the lowest altitudes, the specific mass balance is equal to -5.5 m w.e. In the ablation zone, the mass balance gradient dB/dz is approximately 6 m w.e./yr/km. However, the variation from this rate is high, reflecting differing circumstances across altitude bands. The modelled ELA is approximately at 3060 m altitude. In the accumulation zone, dB/dz lowers to 2 m w.e./yr/km as the ablation approaches zero. Here, the mass balance is dominated by accumulation, which gradually increases with altitude due to the prescribed precipitation gradient and lower temperatures. The total mass balance is -0.80 m w.e./yr.

In Fig. 21(b), the modelled specific mass balance is compared to stake measurements in the lower ablation zone of the Morteratsch glacier by Zekollari & Huybrechts (2018) [19]. In the figure, the line of best fit through these measurements is shown. Direct comparison is not possible because of the time difference between the model and measurements, but it can be instructive of the overall pattern. The measurement line seems to overlap broadly with our modelled specific mass

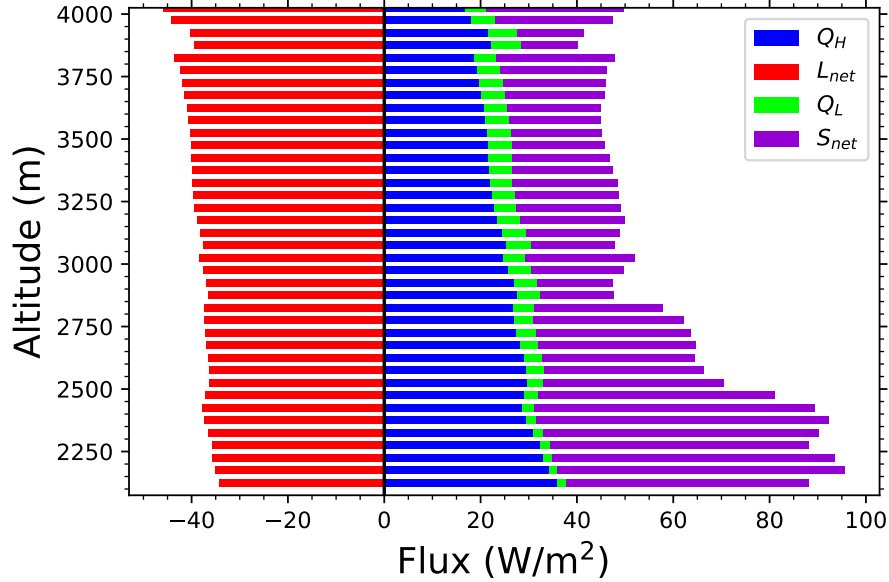


Figure 22: Average modelled energy fluxes for the Ref. run over the period 20 October 2016 to 20 October 2019. Positive values represent fluxes directed towards the surface. The net longwave radiation is obtained by subtracting the outgoing shortwave radiation from the incoming shortwave radiation. Similarly, the net shortwave radiation is the incoming shortwave radiation minus outgoing shortwave radiation.

balance, but shows more divergence at the lowest part of the glacier. From this, it seems possible that the modelled topography effects are too high at the lowest points of the glacier. However, it is important to keep in mind that most measurements by Zekolarri & Huybrechts were in the 2400-2600 m altitude range and that the fit is linear.

The mass balance input of the flow model by Oerlemans et al. [4] is also shown in Fig. 21(b). This function was based on earlier results of the mass balance model by Klok and Oerlemans [4] and measurements of snow accumulation by Sodemann (2006) [18]. The ablation curves correspond well, but there is a large discrepancy in the accumulation zone, where Oerlemans assumes more accumulation at the highest altitudes.

The modelled surface flux distribution in Fig. 22 provides more insight into the distribution of specific mass balance. L_{net} is negative on average, as L_{out} is larger than L_{in} most of the time. It becomes more negative with greater altitudes due to the lower temperature of the atmosphere at these altitudes. The decreasing atmospheric temperature with height also causes a decrease in Q_H with altitude. Q_L increases with altitude due to larger relative humidity at high altitudes. The net shortwave flux varies the most with altitude, reaching values as high as 60 W/m² on the glacier tongue and as low as 20 W/m² in the accumulation zone. Most of this difference can be explained by the albedo differences. Another part of the variation is caused by the differences in slope and topography angle. Overall, the total flux decreases with height. The pattern of the ablation and specific mass balance curve in Fig. 21(a) varying with height returns in the energy balance.

4.4 Model sensitivity

4.4.1 Climate sensitivity

The climate sensitivity of the model to temperature and precipitation was tested by running the model with adjusted temperatures and precipitation rates. The sensitivity tests were conducted over the period 20 October 2016 to 20 October 2019. The results of the climate sensitivity analysis can be seen in Table 3.

A one degree higher atmospheric temperature results in a mass balance of -1,64 m w.e./yr: a decrease of -0,62 m w.e./year with respect to the reference run. The Equilibrium Line Altitude (ELA) changes from 3060 m to 3330 m altitude in this scenario. The decrease in mass balance and increase in ELA is partly related to a decrease in accumulation. The temperature threshold for snowfall is met less often if the temperature increases with 1 K, resulting in 0,11 m w.e./yr less snowfall with respect to the reference run. The decrease in snowfall also causes the albedo to decrease with 0.02, resulting in 2.4 W/m^2 more absorption of solar radiation on average. Q_H and Q_L increase as well, as they are both related to the temperature difference between the glacier and the atmosphere. L_{in} is also related to the atmospheric temperature and increases, but is mostly compensated by an increase in L_{out} as the temperature of the glacier increases as well. A one degree lower temperature causes the ELA to lower to 2860 m and the mass balance to increase with +0,51 m w.e./year. In terms of absolute change, this is lower than the change due to the one degree increase, meaning that the temperature sensitivity is nonlinear. This non linearity partly results from the fact that the absolute difference in snow accumulation is smaller for a temperature decrease, resulting in relatively less mass being added and smaller albedo effects on the shortwave radiation. In addition, the other fluxes also depend on temperature non linearly, changing more when temperature increases.

Increasing the precipitation rate with 10% results in a mass balance increase of 0,15 m w.e./year. Most of the mass balance change is due to the increased snow accumulation. Smaller effects of more snow cover are increased refreezing of water inside the snowpack and a decrease in ablation due to albedo increase. Decreasing the precipitation rate with 10% results in an opposite mass balance change of 0,15 m w.e./year, thus the sensitivity to precipitation is linear. ELA changes are small, in the order of ten meters. This is partly due to the fact that most of the mass balance changes happen in the accumulation zone, where both the amount of precipitation and the ratio of snow to rain are higher than lower on the glacier.

It can be useful to compare these sensitivities to those of Klok's 2D model of the Morteratsch and Pers glacier. We cannot directly compare the results of the models, as they are not identical and Klok models the Morteratsch and Pers glacier together. However, we should expect similar results due to the many similarities between the models. Klok found -0.7 and +0.65 m w.e./yr difference for a temperature change of +1 K and -1 K, and +0,17 and -0,16 m w.e./yr for precipitation changes of +10% and -10%, respectively [12]. Comparing this to the sensitivities we found in Table 3, we find that they are indeed similar.

Table 3: Climate and parameter sensitivity. The first column shows the adjusted parameter or climate conditions with respect to the reference run. The second column shows the yearly mass balance B over the period 20-10-2016 to 20-10-2019 in meters water equivalent per year (m w.e./year). The third column shows the difference in yearly mass balance ΔB between each run and the reference run.

	B (m w.e./year)	ΔB (m w.e./year)
Ref.	-0.80	
T +1 K	-1,42	-0,62
T -1 K	-0,29	+0,51
Prec +10%	-0,65	+0,15
Prec -10%	-0,94	-0,15
t^* +8.9 days	-0,83	-0,17
d^* +9 mm	-0,82	-0,02
α_{ice} +0,05	-0,70	+0,09
f_{topo} +0.1	-0,71	+0,09
f_{topo} -0.1	-0,88	-0,08
b + 0,038	-0,99	-0,20
γ_p +0,2 mm m ⁻¹ yr ⁻¹	-0,55	+0,24
γ_p -0,2 mm m ⁻¹ yr ⁻¹	-1,04	-0,24
No- R	-0,93	-0,14

4.4.2 Parameter sensitivity

The parameter sensitivity of the model is also shown in Table 3. Here, I assessed the parameters that were tuned, namely parameters from the albedo parameterization (t^* , d^* and α_{ice}), the incoming shortwave radiation (f_{topo}), the incoming longwave radiation (b) and the precipitation (γ_P).

Changing t^* from 13 days to its original value of 21.9 days changes the mass balance significantly with -0,17 m w.e./yr. This effect is the largest in the ablation zone. Changing d^* to 31 mm has an effect of only -0,02 m w.e./yr. This effect is so small because d^* is only relevant when the snow layer is thin. Increasing α_{ice} with 0.05 causes an increase in annual mass balance of 0,09 m w.e. The specific mass balance is only sensitive to changes in d^* and α_{ice} in the ablation zone, because above the Equilibrium Line the glacier is covered with snow throughout the year.

The sensitivity to the topography height angle H_{topo} was also assessed, by changing the fraction f_{topo} of the maximum measured topography angle $H_{topo,max}$. The tuned value of f_{topo} is 0.7. There is large uncertainty in this value, as it is tuned only at one altitude despite it is expected to vary over the glacier. An increase of f_{topo} to 0.8 causes the mass balance to increase with +0,09 m w.e./yr. As less radiation reaches the surface when f_{topo} increases, ablation decreases and the mass balance increases. A decrease of f_{topo} with 0.1 causes a decrease of 0,08 m w.e. in the yearly mass balance with respect to the reference run.

The adjustment in longwave radiation also had a big impact on the model outcomes. If the parameter b is adjusted to its initial value 0.433, the emissivity of clear sky increases, resulting in a mass balance change of -0,20 m w.e./yr compared to the reference run.

A change in the precipitation gradient γ_p with 0,2 mm/yr/m causes precipitation to increase with

elevation, increasing the mass balance with 0,24 m w.e./yr. This increase is due to the increased snow precipitation with elevation, which also increases the amount of water that can be refrozen inside the snowpack. A decrease of γ_p with 0,2 mm/yr/m causes the exact opposite: a decrease with 0.24 m w.e./yr.

Of all the adjusted parameters, γ_p and H_{topo} are the most uncertain, because they can only be verified by measurements on the glacier by a limited extent. In addition, the modelled cloud cover is also uncertain, since it is based on measurements 9 and 13 km away from the glacier. However, its sensitivity could not be assessed since it is modelled differently for the incoming shortwave and incoming longwave radiation.

4.4.3 Other sensitivities

Finally, I do a run No-R, where the refreezing of water inside the upper glacier layers is not taken into account. Both the addition of refrozen water to the mass balance and the effects of refreezing on the englacial temperature are turned off. In this case, the yearly mass balance is -0,93 m w.e., or 0,14 m w.e. lower than in the reference run.

5 Experiments and results

5.1 Experiments description

When modelling the impact of artificial snowfall on the glacier, there are several different settings to consider. The most important ones are where to add snow and the effect of possible water availability constraints. All experiments are listed in Table 6. All experiments are compared to the Reference run, where no artificial snow is added.

In the first experiment Exp-TOT, I examine the situation in which there is unlimited water supply and it snows on the whole glacier. This is done to get an indication of the impact of the artificial snow on different locations on the glacier.

As the next step, I perform an experiment Exp-basic where the artificial snow is limited to an 0.81 km² area between 2415-2505 m altitude, called the basic area. This area roughly corresponds to the area used by Oerlemans in 2017 [4], that is favored due to the topography and position in the ablation zone. The water supply is still unlimited.

In the third experiment I consider how slight changes to the area chosen above affect the results. I adjust the upper altitude of the basic area, resulting in a smaller area of 0.50 m² and a bigger area of 1.01 m². The experiments where I let it snow only in these areas with unlimited water supply are called Exp-big and Exp-small, respectively.

I model extreme water availability constraints for supplying snow to the 0.81 km² area. I model water limitation by creating a reservoir in the model. As input for the reservoir, a fraction of 31% of the total meltwater of Morteratsch every hour is used. Every time step that Morteratsch glacier melts, that melt is added to the reservoir. When conditions are right for snow and the reservoir contains enough water, snow is supplied to the surface and the amount of water in the reservoir is adjusted. I did three different runs with reservoir sizes of 10⁴, 10⁵ and 10⁶ m³.

In all these experiments, results are evaluated from the 20th of October 2016 until the 20th of October 2019. Artificial snow is only added when $T_{wb} < -2$ °C. If all conditions for artificial snow are met, it is added at a rate of 1.2 mm w.e./hr.

The results depend on these assumptions. The sensitivity to the assumptions is evaluated by doing sensitivity runs with slightly different settings. All of these runs are variations on the Exp-basic run. To evaluate the sensitivity to snow starting time, I do an additional run from the 1st of July 2016 to the 1st of July 2019. I also do a run where I let it snow only in the months high glacier ablation, namely June, July, August and September. For the T_{wb} limit, I do two separate runs where the limit is raised and lowered by one degree. Further tests include varying the artificial snow rate in a few runs. Finally, I do the same climate sensitivity test as I did for the reference run and compare the results.

5.2 Results

5.2.1 Height dependence on artificial snow effects

In the first experiment, artificial snow is supplied to the whole glacier without water limitations. In Fig. 23(a), the yearly artificial snow accumulation ΔP is shown as a function of altitude. ΔP increases roughly linearly from around 4.5 to 8.3 m w.e./yr with increasing altitude. This is due to the fact that T_{wb} criterion is met more often at higher glacier altitudes, where the average

Table 4: Description of all experimental runs.

Run	Description
Reference	Normal conditions without artificial snow
Exp-TOT	Artificial snow on whole glacier without constraints
Exp-basic	Artificial snow in basic area of 0.81 m ² near AWS
Exp-big	Artificial snow in bigger area of 1.01 m ² near AWS
Exp-small	Artificial snow in smaller area of 0.50 m ² near AWS
Exp-JJAS	Artificial snow in basic area only in the months June, July, August and September
Exp-Res10 ⁴ m ³	Artificial snow in basic area, constrained by a reservoir of 10 ⁴ m ³
Exp-Res10 ⁵ m ³	Artificial snow in basic area, constrained by a reservoir of 10 ⁵ m ³
Exp-Res10 ⁶ m ³	Artificial snow in basic area, constrained by a reservoir of 10 ⁶ m ³

temperature is lower. On the highest altitudes of the glacier artificial snow can be supplied 75% of the time, on the lowest altitudes 37% of the time.

Fig. 23(a) also shows the change in mass balance ΔB of the experimental run with respect to the reference run. ΔB is positive over the whole glacier, indicating an increase in mass balance with respect to the reference run. ΔB varies around 7-7.5 m w.e./yr in the ablation zone, and increases to 8.5 m w.e./yr at the top of the glacier. The total mass balance is 6.74 m w.e./yr when artificial snow is supplied to the whole glacier without water limitations.

The size of the indirect effect of artificial snow is indicated by the mass balance factor $F_{MB} = \Delta B / \Delta P$. This factor is plotted as a function of height in Fig. 23(b). F_{MB} is around 1 at the top half of the glacier. Below 2900 m altitude it increases to a 1.6 maximum at the lower glacier tongue. This indicates that the impact of artificial snow deposition increases with lower glacier altitude. Artificial snow is most effective at lower altitudes because the albedo can increase more in the ablation zone, resulting in a feedback effect where more solar radiation is reflected and melt is reduced.

5.2.2 Effects of snow on selected area

When artificial snow is added only in the 0.81 km² area without taking into account water limitations, on average $4.38 \cdot 10^9$ kg of water is used for snow production every year. As can be seen in Fig. 24(a), in the first balance year the snow depth reaches a maximum of around 15 meters. In the following years, the snow layer becomes even thicker because not everything melts away during the melt seasons. Most of the snow cover is gained through the addition of artificial snow in winter.

The presence of constant snow cover has a big impact on the albedo, as can be seen in Fig. 24(b). The modelled albedo is almost always at the maximum value of 0.9 in winter due to the frequent artificial snowfall. During the summer, the albedo varies more, also interannually. Furthermore, the albedo is always above 0.53, the lowest albedo for snow (α_{firn} in Eq. 13). This is a big difference with the normal situation, where the summer albedo is equal to the ice albedo of 0.3 most of the time. On average, the albedo in the artificial snow area is 0.66 in the reference run and 0.82 in the experimental run.

The impact of the albedo change can also clearly be seen in Fig. 25(b), where the fluxes in

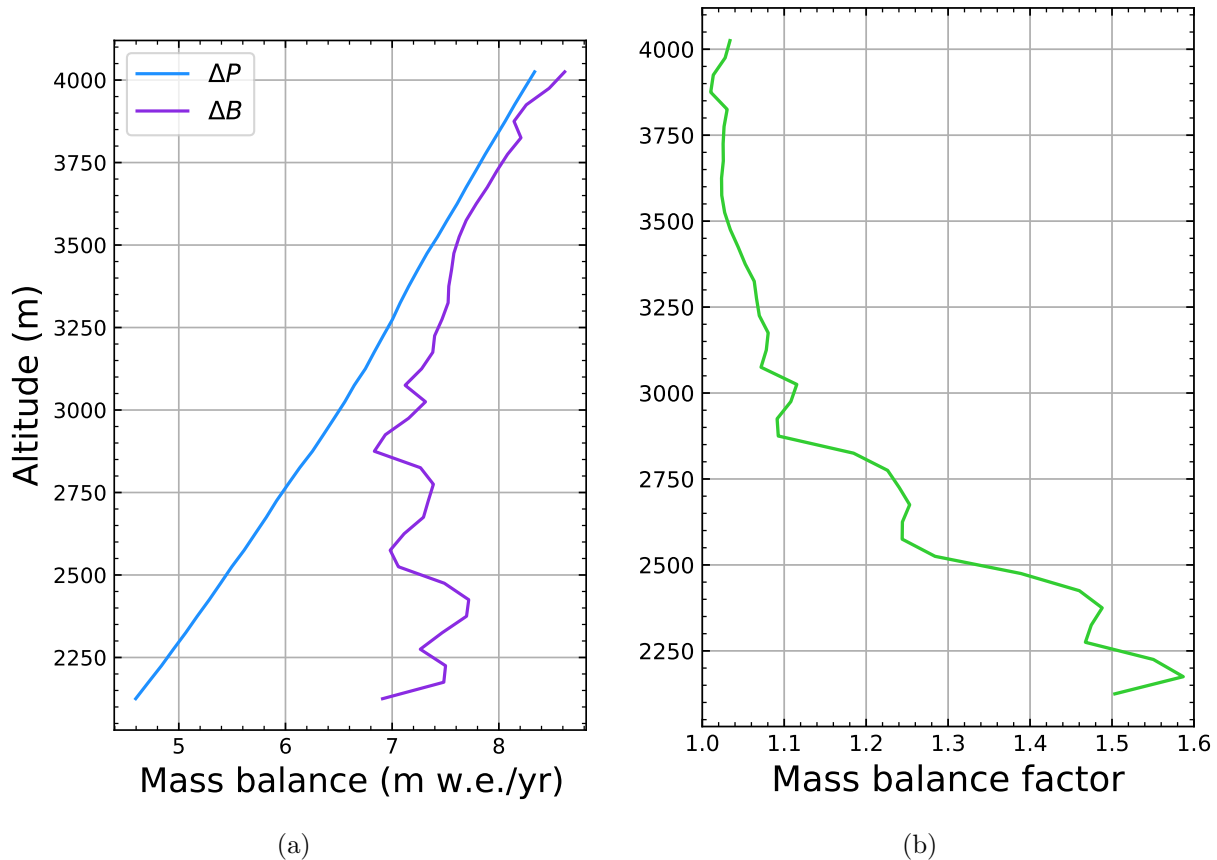


Figure 23: (a) Effects of snow suppletion on the yearly accumulation and mass balance as a function of height. The blue line shows the total yearly artificial snow accumulation ΔP . The purple line shows the difference in yearly mass balance ΔB between the experimental run and the reference run. (b) Mass balance factor as a function of height. The mass balance factor is calculated by dividing the total mass balance change by the total accumulation change.

the artificial snow area are compared to the reference run. Due to the increased albedo, the net shortwave radiation is 24.3 W/m^2 lower. The net longwave radiation is less negative, due to the upper glacier layer being 0.6 K colder in the experiment. The temperature change also results in slightly larger turbulent fluxes. Overall, a change of -18.2 W/m^2 in surface flux is achieved.

In Fig. 24(c) the specific mass balance over time is plotted for the artificial snow area. The experimental run is compared to the reference run. A large increase in the mass balance is visible during winter, when most of the artificial snow accumulates. The mass balance is less negative during summer with respect to the reference run. This effect decreases over the years, as the average albedo decreases as well. In Fig. 24(d), the weekly difference in mass balance ΔB between the experimental run and reference run is separated into the change in accumulation ΔP and the indirect change $\Delta B - \Delta P$. From this figure, it becomes clear that the vast majority of artificial snow is supplied during accumulation season, and that the indirect effects occur mostly during summer.

In Fig. 25(a), the modelled specific mass balance after artificial snow over the specific area is shown. The total mass balance with artificial snow deposition is $+0.14 \text{ m w.e./yr}$, a $+0.93 \text{ m w.e./yr}$ increase with respect to the reference run. As expected, this is much less than the $+6.74$

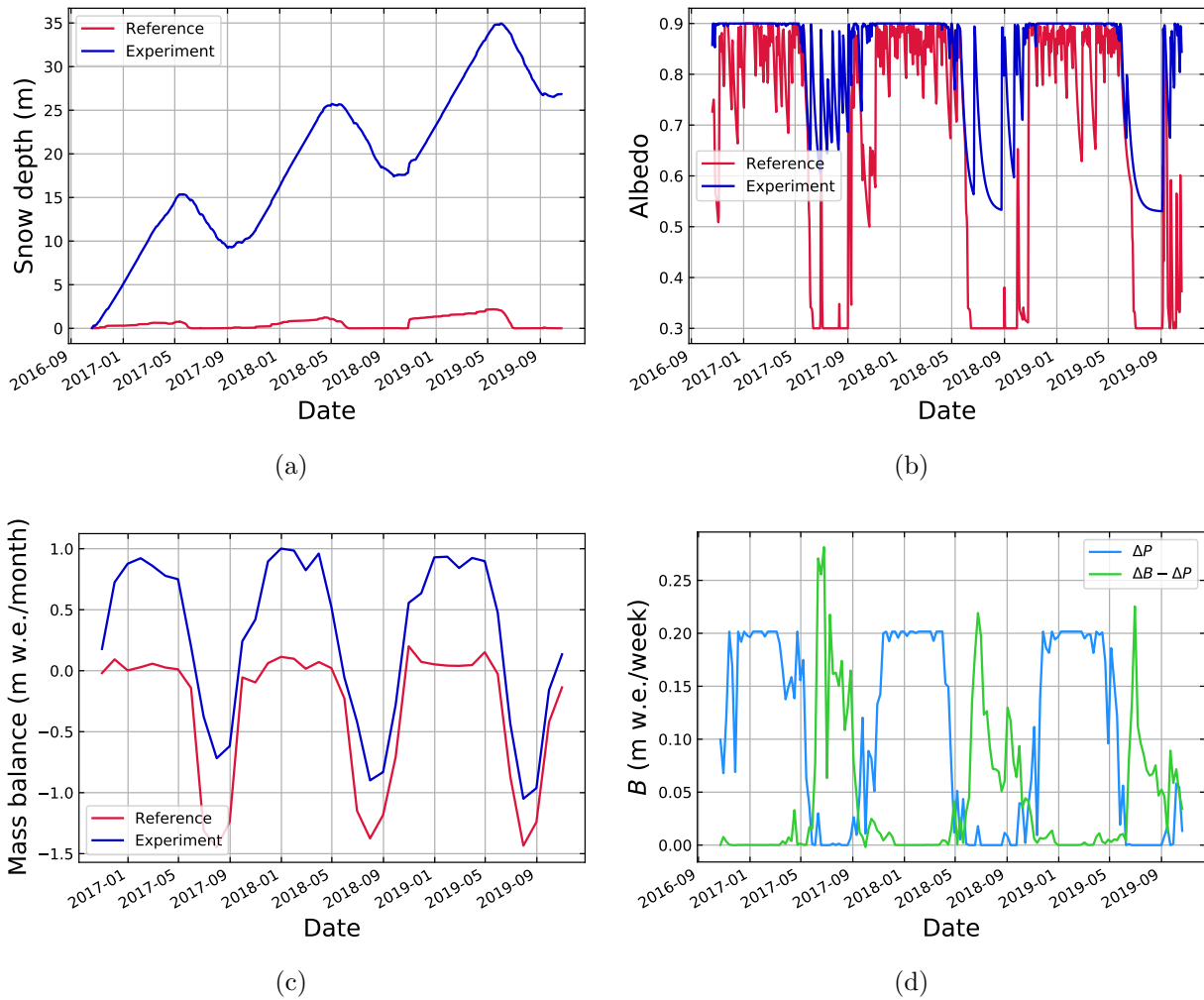


Figure 24: Model outcomes at the area covered with artificial snow, weighted over elevation bands. In (a), (b) and (c) the snow depth, daily average albedo and monthly mass balance are shown for the experimental run (blue) and the reference run (red). (d) shows the change in weekly mass balance with respect to reference run. The change in accumulation ΔP is shown by the light blue line. The rest of the mass balance change $\Delta B - \Delta P$ is shown by the green line.

m w.e./yr that could theoretically be achieved when artificial snow is supplied to the whole glacier.

5.2.3 Area variability

The area that can be covered with artificial snow depends on total meltwater availability and practical constraints. In table 5, the results of runs with adjusted areas are shown. For all areas, the lower boundary is kept at 2415 m, just above the altitude where the Pers glacier ends. For Exp-small, the upper boundary is lowered to 2480 m altitude, resulting in an area of 0.5 km². Covering this area with snow achieves an increase of +0.71 m w.e./yr with respect to the reference run, resulting in a total mass balance of -0.09 m w.e. For Exp-large, the upper boundary is moved to 2600 m, which is likely not feasible in reality. It results in an area of 1.0 km² that can be covered. The resulting mass balance is +0.35 m w.e./yr.

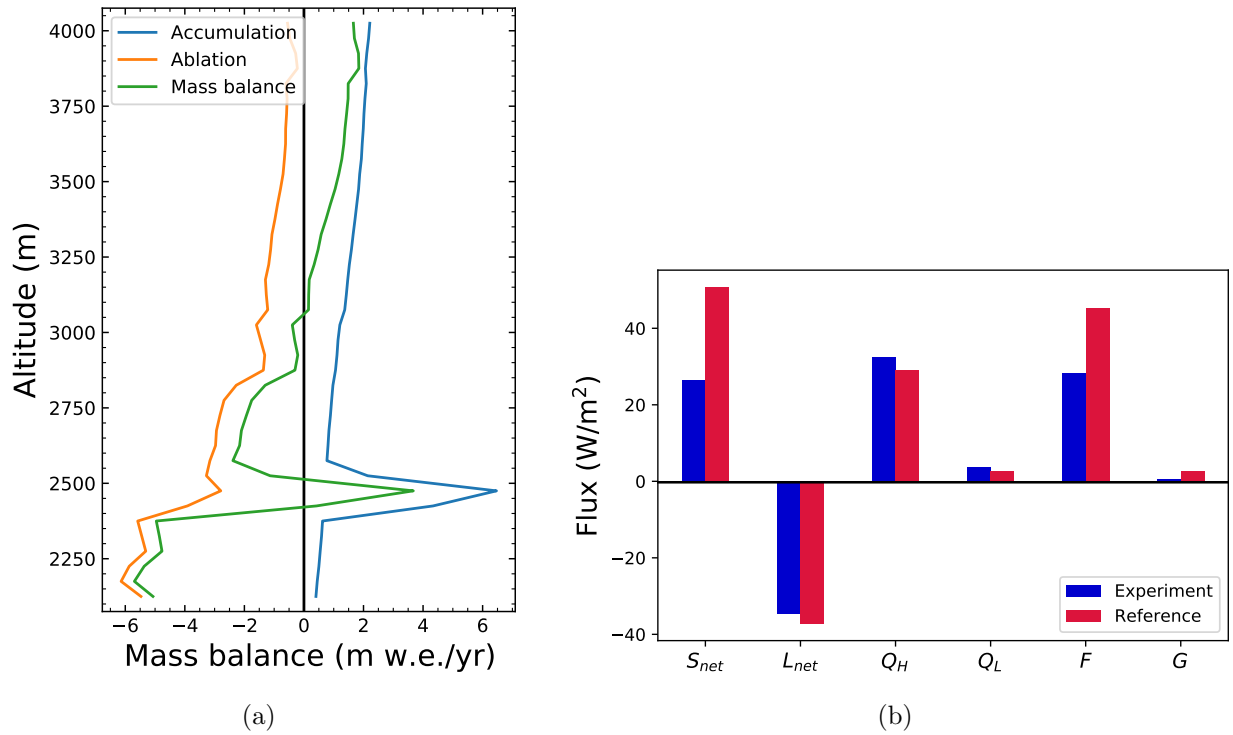


Figure 25: (a) Yearly average mass balance for unlimited snow supply to the basic area. (b) Average fluxes at artificial snow area, weighted over altitude bands. The fluxes in the reference run (red) are compared to the fluxes in the Exp-basic run (blue).

Table 5: Altitude range, area, mass balance and mass balance factor for three different areas.

	Altitude range (m)	A_{snow} (km ²)	B (m w.e./year)	F_{MB}
Reference	-	-	-0.80	-
Exp-basic	2415-2505	0.81	+0.14	1.40
Exp-small	2415-2480	0.50	-0.09	1.41
Exp-large	2415-2600	1.01	+0.35	1.37
Exp-TOT	2125-4000	6.53	+6.74	1.14

Table 5 also shows the mass balance for Exp-TOT, which was discussed in Section 5.2.1.

5.2.4 Water availability constraints

In the Exp-basic run without water limitations, on average $4.38 \cdot 10^9$ kg of water per year is used for artificial snow production. An order estimate of the available Pers meltwater can be obtained from the Morteratsch meltwater. It is estimated that around a quarter of the meltwater from the Pers glacier can be used for artificial snow production. The annual Morteratsch meltwater is $1.4 \cdot 10^{10}$ kg/yr, around three times as much as the needed water for artificial snow. Assuming that the Morteratsch glacier and Pers glacier produce roughly the same amount, the majority of the used water in the Exp-basic run could be provided by meltwater from the Pers glacier.

However, the water can only be provided if it is stored somewhere. Glacier runoff varies greatly throughout the year. In Fig. 26(a), the monthly runoff of the Morteratsch glacier above 2500 m is plotted together with the amount of water needed for maximum artificial snow deposition in the

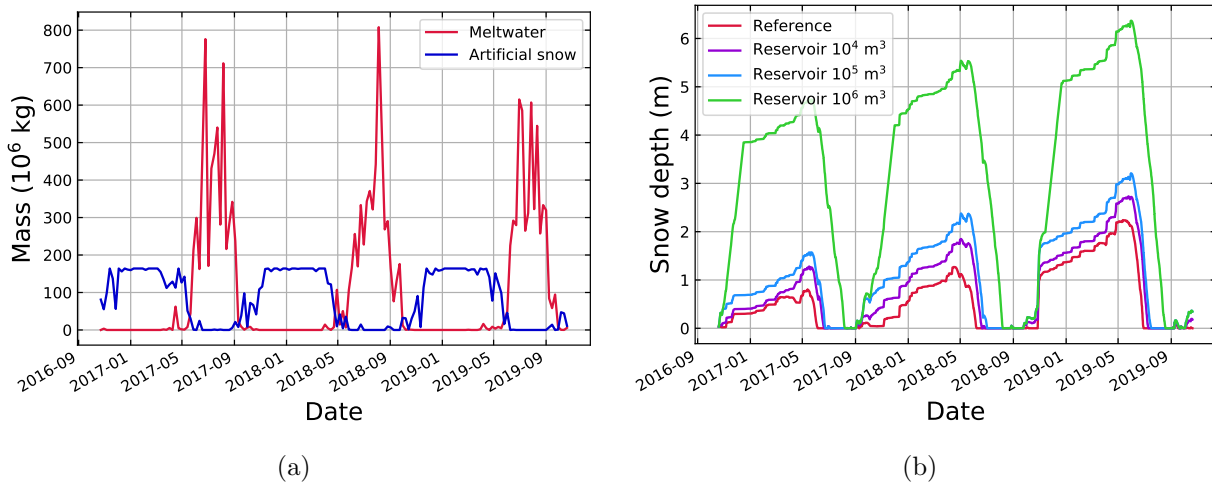


Figure 26: (a) The blue line shows the weekly supplied artificial snow mass for the Exp-basic run. The red line shows the weekly summed melt at Morteratsch glacier above 2500m. (b) Snow depth at 2475 m for different sizes of the meltwater reservoir. Snow depths for reservoir sizes of 10^4 m³ (purple line), 10^5 m³ (blue line) and 10^6 m³ (green line) are shown. The reference snow depth is shown by the red line.

0.8 km² area. Snow can most often be supplied in winter whereas melt takes place only in the ablation season. This indicates that water availability doesn't match up with water demand in time.

To assess the effect of a limited storage of water, I did three runs with different reservoir sizes 10^4 m³, 10^5 m³ and 10^6 m³. The reservoir of 10^4 m³ can contain enough water to supply the basic area with artificial snow for around 10 hours. The reservoir of 10^6 m³ can contain almost a quarter of the needed water for a year of unlimited snow supply at the basic area. In Fig. 26(b), the snow depths resulting from supply at 2475 m altitude are shown. For all of the reservoir sizes, snow cover cannot be maintained throughout the year. However, the period of maintained snow cover is significantly longer than in the reference run, especially in the case of the 10^6 m³ reservoir. In Table 6, the resulting mass balances are shown. In the case of the 10^4 m³ reservoir, only 0.03 m w.e./yr of artificial snow can be supplied to the surface, resulting in a mass balance of -0.68 m w.e./yr, a difference of +0.11 m w.e./yr with the reference run. For a 10 times bigger reservoir, a mass balance of -0.64 m w.e./yr is obtained. When a reservoir of 10^6 m³ is used, the mass balance can be increased to -0.42 m w.e./yr. The mass balance factor F_{MB} is bigger when smaller reservoirs are used, reflecting higher effectiveness of lesser amounts of snow supply.

5.2.5 Snow supply sensitivity

In Table 6, sensitivities in the snow supply are shown as well. In all of these runs, snow is supplied in the basic area and unlimited water is available. First, the sensitivity of the artificial snow rate of 1.2 mm w.e./hr is considered by looking at effects of changing it by 10%. A 10% higher and lower artificial snow supply rate changes the mass balance with +0.07 and -0.07 m w.e./yr, respectively. The mass balance factor F_{MB} decreases somewhat for a higher rate, indicating that additional artificial snow has a lower impact. In Fig. 27(a), more variations on the snow supply rate are shown with their effects on the mass balance change. ΔB increases with increased snow supply

Table 6: Effects of snow supply variability in area A on the mass balance B , mass balance change with respect to the reference run ΔB , artificial snow supply ΔP and the mass balance factor F_{MB} .

	B (m w.e./yr)	ΔB (m w.e./yr)	ΔP (m w.e./yr)	F_{MB}
Reference	-0.80	-	-	-
Exp-basic	+0.14	+0.93	+0.67	1.40
Exp-Res 10^4m^3	-0.68	+0.11	+0.03	4.05
Exp-Res 10^5m^3	-0.64	+0.15	+0.05	2.87
Exp-Res 10^6m^3	-0.42	+0.38	+0.19	1.97
T_{wb} cut off = -1 °C	+0.23	+1.02	+0.73	1.40
T_{wb} cut off = -3 °C	+0.05	+0.85	+0.61	1.40
Artificial snow +10%	+0.20	+1.00	+0.74	1.36
Artificial snow -10%	+0.07	+0.78	+0.60	1.44
Start 1-7	+0.15	+0.91	+0.68	1.36
Exp-JJAS	-0.74	+0.06	+0.01	4.00

rate. At very low supply rates, the effect on ΔB is nonlinear. From 0.12 to 0.48 mm w.e./hr, the relationship between supply rate and ΔB is approximately linear. An increase in artificial snow rate has a mass balance factor of 1.6. An inflection point is visible at 0.48 mm w.e./hr. This rate corresponds to the rate at which snow cover cannot be maintained in the elevation band 2450-2500 m, which is the most prominent band in the basic area. Above this point, F_{MB} is equal to 1.03. The snow supply rate could potentially be a lot higher than the assumed rate of 1.2 mm w.e. per hour, as artificial snow production increases with lower wet bulb temperature. From wet bulb temperatures below -7 °C, the snow showers can produce four times as much snow. Therefore, we would expect the artificial snow deposition to be even higher in winter if there are no water supply limitations. In practice, the amount of snow needed for the basic experiment is already quite high and comparable in magnitude to the maximum expected available melt water.

Secondly, the effect of a change in wet bulb temperature cut off for artificial snow is considered. A increase of the cut off wet bulb temperature to -1 °C results in more artificial snow being deposited and an increase of the mass balance with +0.09 m w.e./yr with respect to the experimental run. When T_{wb} is lowered with one degree, the opposite effect takes place, and the mass balance decreases with 0.09 to +0.05 m w.e./yr. The mass balance factor F_{MB} is 1.4 in both cases, indicating that the snow that is supplied is equally effective.

Additionally, a the run Exp-JJAS is done where artificial snow can only be supplied in the summer months June, July, August and September. In this case, only 0.01 m w.e. artificial snow can be supplied per year. The effectiveness of the snow is high, however, as the mass balance change due to the snow is equal to +0.06 m w.e. This run is quite similar in characteristics to the reservoir run of 10^4m^3 .

Finally, I consider starting with artificial snow deposition at the 1st of July instead of the 20th of October 2016. This gives roughly similar results to the Exp-basic run, despite the fact that in this case snow cover cannot be maintained in the first months. Apparently, the variations in weather are larger than the effect of decreased snow cover.

Table 7: Climate sensitivity of results. The mass balance change ΔB and precipitation change ΔP are calculated with respect to the reference runs with the same climate adjustment.

	B (m w.e./yr)	ΔB (m w.e./yr)	ΔP (m w.e./yr)	F_{MB}
Exp. run	+0.14	+0.93	0.67	1.40
T +1 K	-0.53	+0.88	0.61	1.44
T -1 K	+0.69	+0.98	0.73	1.35
Prec +10%	+0.28	+0.93	0.67	1.39
Prec -10%	+0.00	+0.94	0.67	1.41

5.2.6 Climate sensitivity

As a final experiment, the sensitivity of the results to climate changes was tested. In table 7, the climate sensitivities are shown. When the temperature is increased by 1 K, the reference mass balance is already lower (-1,64 m w.e./yr), as we saw in Table 3. In addition, the higher temperatures make artificial snow deposition more difficult. This results in a somewhat lower mass balance change of +0,88 m w.e./yr, which brings the yearly mass balance with artificial snow to -0.53 m w.e. under these conditions.

A one degree lower temperature has the opposite effect, with artificial snow changing the mass balance to +0.69 m w.e./yr. In Fig. 27(b), the monthly mass balance is shown for the different temperature runs. A clear difference in ablation is visible between the different runs.

Changes in precipitation on the order of 10% affect the annual mass balance significantly, but the effects of artificial snow are similar to the experimental run under normal climatic conditions.

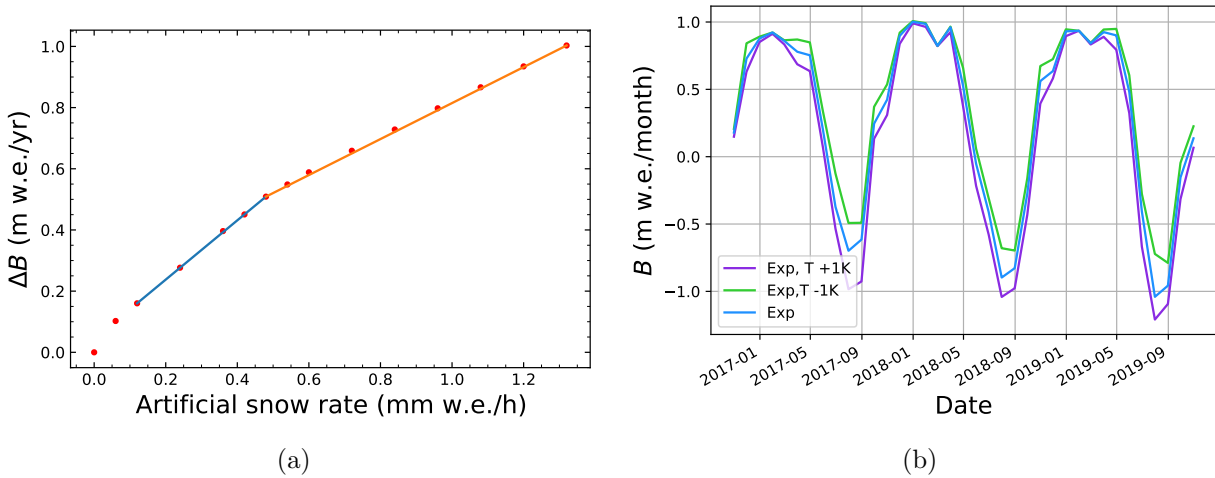


Figure 27: (a) The mass balance change with respect to the reference run for artificial snow supply in the basic area at different rates. Each dot represents a run. Lines are drawn between the points where a linear effect is visible. (b) Monthly mass balance at artificial snow area for temperature variations, averaged over height bands. The results of increasing the temperature by 1K (purple line) and decreasing the temperature by 1K (green line) are shown. The blue line shows Exp-basic, the experiment under unchanged climatic conditions.

6 Conclusions, discussion, and outlook

6.1 Key assumptions and model improvements

In the mass balance modelling, a main uncertainty is the modelling of the shortwave radiation. The topography angle was estimated by multiplying the maximum topography angle for each height by 0.7, which was tuned to the AWS observations. This approach is risky. A more sophisticated way of estimating the topography angle would include a 2D model using a Digital Elevation model. Other uncertain factors are the precipitation gradient and the cloud cover. Just like for the topography angle, the evaluation data is limited for these parameters.

There additional uncertainties related to the modelling of the snowpack. When large amounts of artificial snow are added to the model some of these uncertainties become larger. For example, the model is stationary, whereas the glacier itself is not. The glacier surface near the AWS moves with 50 meters per year on average. As a result, the modelled snow depth over multiple years is not entirely realistic. This is especially the case for modelled artificial snowfall, since a part of the glacier surface moves in and later out of the artificial snow accumulation area. This gives a slight advantage when more snow than needed to cover the ice for one year is supplied to the surface.

More uncertainties arise from the snow density modelling. The model uses a stationary density distribution with snow depth, and thus densification of snow is not taken into account. (The snow density is for example used to model the amount of water that refreezes inside the snow layer.) As a result of the flawed density modelling, the modelled snow depth deviates significantly from the measured snow depth. This gives another reason why modelled snow depth for artificial snow experiments should not be relied too much upon. The snow density modelling is likely not a big problem for the albedo, since the snow mass is probably modelled better. When the snow mass is modelled correctly, the timing of the snow pack melt will be correct. Very small snow depths are an exception here, as they determine the difference between snow and ice albedo. The albedo parameterization itself also provides uncertainty for the artificial snow runs, as the parameterisation is based on regular amounts of snowfall. Ideally, albedo modelling would take into account how old the snow at the surface is, which could perhaps be possible if the density was modelled in a similar way. The age of the upper snow is approximated with the time since last snowfall in the modelling, but for large amounts of snowfall, the upper snow will on average be fresher than for smaller amounts of snowfall.

Finally, in the model it was assumed that all applied artificial snow would spread evenly and that no snow would blow away from the glacier. The sensitivity to these variations depends on how much snow is already supplied to the surface. When a full snow cover is maintained throughout the year, the changes in mass balance are mostly due to the direct effects of snowfall, except when the area is close to the tipping point of total snow cover. For an area with less snow, changes in snowcover are more impactful since albedo effects play a role as well.

6.2 Main conclusions and future research

I found that the effects of artificial snowfall vary a lot over the Morteratsch glacier. Higher up the glacier more snow can be deposited and snow cover is maintained longer. However, the indirect effect of a snow cover is much higher in the ablation zone, especially below 2500 m altitude.

The due to practical constraints favoured area from 2415-2505 m is thus also favourable in terms of 'snow efficiency', although lower areas are even better. With no water constraints, it is possible to increase the mass balance of the Morteratsch glacier from -0.80 to +0.14 m w.e./yr. Under this scenario, $4.38 \cdot 10^9$ kg water is used for artificial snow, of which around half melts away after every year.

An increase in temperature decreases the amount of snow that can be deposited, but for a one degree increase in temperature snow cover can still easily be maintained. Due to increased ablation, the total mass balance will be much lower.

The amount of water needed for artificial snow cover is large, and it might not be possible to store that amount. In the scenario where only 10^4 m³ of water can be stored, the mass balance is -0.68 m w.e./yr. For a 100 times larger reservoir of 10^6 m³, the mass balance increases to -0.42 m w.e./yr.

To get a better estimation of the total available meltwater, a model of Pers glacier can be used to calculate the melt expected to fill the meltwater lake. The timing of the melt of Pers glacier will probably correspond to the modelled Morteratsch melt, but the amount of meltwater is less certain.

References

- [1] H.-O. Portner, D. Roberts, V. Masson-Delmotte, P. Zhai, E. Poloczanska, K. Mintenbeck, M. Tignor, A. Alegria, M. Nicolai, A. Okem, J. Petzold, B. Rama, and N. Weyer, “Summary for policymakers.” IPCC Special Report on the Ocean and Cryosphere in a Changing Climate, 7 2019. In press.
- [2] H.-O. Portner, D. Roberts, V. Masson-Delmotte, P. Zhai, E. Poloczanska, K. Mintenbeck, M. Tignor, A. Alegria, M. Nicolai, A. Okem, J. Petzold, B. Rama, and N. Weyer, “Technical summary.” IPCC Special Report on the Ocean and Cryosphere in a Changing Climate, 7 2019. In press.
- [3] “Glamos: Glacier monitoring switzerland: Vadret da morteratsch.” URL: <https://www.glamos.ch/en/mapviewer/E22%2F03>. Accessed 06/01/2021.
- [4] J. Oerlemans, M. Haag, and F. Keller, “Slowing down the retreat of morteratsch glacier, switzerland, by artificially produced summer snow: a feasibility study,” *Climatic Change*, pp. 189–203, 2017.
- [5] J. Oerlemans and L. Klok, “Effect of summer snowfall on glacier mass balance,” *Annals of Glaciology*, vol. 64, pp. 97–100, 2004.
- [6] J. Oerlemans, R. Giesen, and M. van den Broeke, “Retreating alpine glaciers: increased melt rates due to accumulation of dust (vadret da morteratsch, switzerland),” *Journal of Glaciology*, no. 192, pp. 729–736, 2009.
- [7] J. Oerlemans, *The Microclimate of Valley Glaciers*. Utrecht: Igtur, Utrecht Publishing & Archiving Services, Universiteitsbibliotheek Utrecht, 2010.
- [8] R. Pravettoni, “Picture: Glacier mass balance,” 2021. URL: <https://www.grida.no/resources/12826>, Accessed 15/01/2021.
- [9] C. Seupel. Hypsometry of Morteratsch glacier (personal communication).
- [10] J. Oerlemans, “Can the retreat of the morteratsch glacier be stopped?,” 2016. URL: <https://www.uu.nl/en/news/can-the-retreat-of-the-morteratsch-glacier-be-stopped>, Accessed 06/01/2021.
- [11] J. Oerlemans and E. J. Klok, “Energy balance of a glacier surface: Analysis of automatic weather station data from the morteratschgletscher, switzerland,” *Arctic, Antarctic, and Alpine Research*, 2002.
- [12] L. Klok and J. Oerlemans, “Model study of the spatial distribution of the energy and mass balance of morteratschgletscher, switzerland,” *Journal of Glaciology*, no. 163, pp. 505–518, 2002.
- [13] “Mortalive: Technology.” URL: <https://mortalive.com/technology>. Accessed 06/01/2021.
- [14] “Bachler: Nussy zeroe.” URL: <https://www.bachler.ch/en/Snowmaking/NESSy-ZeroE>. Accessed 06/01/2021.
- [15] “Karten der schweiz.” URL: <https://map.geo.admin.ch/>. Accessed 06/01/2021.

-
- [16] B. Ding, K. Yang, J. Qin, L. Wang, Y. Chen, and X. He, “The dependence of precipitation types on surface elevation and meteorological conditions and its parameterization,” *Journal of Hydrology*, pp. 154–163, 2014.
- [17] M. Schwarb, *The alpine precipitation climate: evaluation of a high-resolution analysis scheme using comprehensive rain-gauge data*. PhD thesis, ETH Zürich, Zürich, 7 2000. Diss. ETH No, 13911.
- [18] H. Sodemann, A. S. Palmer, C. Schwierz, and M. S. and H. Wernli, “The transport history of two saharan dust events archived in an alpine ice core.,” *Atmospheric Chemistry and Physics Discussions, European Geosciences Union*, 2005.
- [19] H. Zekollari and P. Huybrechts, “Statistical modelling of the surface mass-balance variability of the morteratsch glacier, switzerland: strong control of early melting season meteorological conditions,” *Journal of Glaciology*, vol. 64, pp. 275–288, 2018.